NREL/TP-441-6913 • UC Category: 1211 • DE95004034

Experimental Investigation of Aerodynamic Devices for Wind Turbine Rotational Speed Control

Phase 1

L. Scott Miller, Ph.D.
Wichita State University
Wichita, Kansas

NREL Technical Monitor: Paul G. Migliore

National Renewable Energy Laboratory
1617 Cole Boulevard
Golden, Colorado 80401-3393
A national laboratory of the U.S. Department of Energy
Managed by Midwest Research Institute
for the U.S. Department of Energy
under contract No. DE-AC36-83CH10093

Prepared under Subcontract No. XAD-3-133365-01

February 1995

NOTICE

Available to DOE and DOE contractors from:
Office of Scientific and Technical Information (OSTI)
P.O. Box 62
Oak Ridge, TN 37831
Prices available by calling (615) 576-8401

Available to the public from:
National Technical Information Service (NTIS)
U.S. Department of Commerce
5285 Port Royal Road
Springfield, VA 22161
(703) 487-4650

Printed on paper containing at least 50% wastepaper and 10% postconsumer waste

Foreword

The Wind Technology Division of the National Renewable Energy Laboratory (NREL) is conducting exploratory research on aerodynamic devices that are intended to enhance wind turbine rotor performance and attenuate structural loads. Desired properties of these devices include simplicity, reliability, maintainability, low cost, and fail-safe design. Initial efforts have focused on the use of trailing-edge aerodynamic brakes for overspeed protection. Long-term efforts will address more aggressive and innovative strategies that have the potential to significantly advance the state-of-the-art.

This report touches on the work performed in two projects: Subcontract No. TAD-3-13400 "Wind Turbine Trailing-Edge Aerodynamnic Brake Design" performed by Gene A. Quandt, and Subcontract No. XAD-3-133365 entitled "Aerodynamic Devices for Wind Turbine Performance Enhancement" performed by Wichita State University (WSU). These two projects progressed in parallel, with considerable interaction between the principal investigators.

The WSU Phase-1 Report discussed the configurations studies and the attempts to identify promising alternatives through the analysis of the wind tunnel test data. The Phase-2 Report is currently in preparation. It presents wind tunnel results for "spoiler flaps" of 30% and 50% chord; for various leading-edge lip extensions; and for different gap sizes. Gene Quandt's subcontract report, which is currently being edited, focuses on aerodynamic and structural design, and includes preliminary design calculations for a centrifugally-actuated aerodynamic brake.

As is often the case with exploratory research endeavors, these projects have spawned additional follow-on studies. Wind tunnel tests are planned at Ohio State University (OSU) in which a pressure-tapped S809 airfoil model will be tested with three trailing-edge devices: the spoiler flap, a plain flap ("unvented aileron") and a vented plain flap ("vented aileron"). Rotating blade tests of these same confiurations will be conducted at the National Wind Technology Center (NWTC), with the goal of quantifying the effects of unsteadiness, blade rotation and aspect ratio, so that corrections can be applied to wind tunnel test data for use by wind turbine designers in the future.

Paul G. Migliore, Technical Monitor

Preface

The work performed and presented in this report is the product of a group effort. Special thanks and recognition go to Paul Migliore, from the National Renewable Energy Laboratory (NREL), and Gene A. Quandt, from Colorado State University (CSU). Paul's technical help and program guidance have been outstanding, constructive, and most welcome. Gene Quandt deserves special recognition for skillfully identifying four new turbine trailing-edge controls that offer great promise. In addition, Northern Power Systems provided a great deal of help and advice as the project developed. Their contributions and suggestions are much appreciated. Wichita State University (WSU) machine shop and wind tunnel personnel did an exceptional job building and testing the models. Art Porter and Bonnie Johnson did an outstanding job. Two of my graduate students, Steve Huang and Ihssane Mounir, worked long and hard preparing for the tests, helping with the work, and reducing the data. They did an exceptional job and learned a great deal. Special thanks go to the many other WSU students (Ziad, Jim, Boyd, Scott, Mark, Tram, and Jen) who worked on the project. My good friend and colleague, Dr. Michael Papadakis, provided valuable technical feedback on this report and many ideas for future activities. I want to thank everyone involved, including the U.S. Department of Energy (DOE) and NREL, for their support.

Summary

An investigation was undertaken to identify the aerodynamic performance of five separate trailing-edge control devices, and to evaluate their potential for wind turbine overspeed and power modulation applications. A modular two-dimensional wind tunnel model was constructed and evaluated during extensive wind tunnel testing. Aerodynamic lift, drag, suction, and pressure coefficient data were acquired and analyzed for various control configurations and angles of attack. To further interpret their potential performance, the controls were evaluated numerically using a generic wind turbine geometry and a performance analysis computer program. Results indicated that the Spoiler-Flap control configuration was best suited for turbine braking applications. It exhibited a large negative suction coefficient over a broad angle-of-attack range, and good turbine braking capabilities, especially at low tip-speed ratio.

Contents

Nomenclature

c	Airfoil chord, including the control
c_c	Control chord
L	Section lift, per unit span, acting perpendicular to approach flow direction
D	Section drag, per unit span, acting parallel to approach flow direction
M_c	Section control hinge moment, per unit span, positive is clockwise
C_l	Section lift coefficient = $(L)/[(q)(c)]$
C_d	Section drag coefficient = $(D)/[(q)(c)]$
C_q	Total turbine rotor torque coefficient = $(Q)/[1/2(\rho)(\Pi R^2)(\Omega R)^2(R)]$
C_s	Section suction coefficient = $(C_l)(\sin \alpha) - (C_d)(\cos \alpha)$
Cm_h	Control-hinge moment coefficient = $(M_c)/[(q)(c_c^2)]$
Q	Total turbine rotor torque
q	Dynamic pressure = $(0.5)(\rho)(V^2)$
R	Rotor radius
R_c	Reynolds number = $[(V)(\rho)(c)]/(\mu)$
V	Relative inflow velocity
V_W	Wind velocity
X	Tip-speed ratio = $(\Omega R)/V_W$
α	Airfoil angle of attack, nose up is positive
δ	Trailing-edge device deflection angle, trailing edge down is positive
μ	Absolute viscosity of air
Ω	Rotor rotational speed
ρ	Mass density of air

Introduction

Turbine Power Modulation and Braking

Over the ages, wind turbines have been used to extract energy from the wind. Interest in the use of these devices has increased the last decade because of the need for safe and renewable energy. Unfortunately, wind turbine use has been limited in some cases by such factors as consistent power production, component durability, system maintainability, and operating costs. Recent improvements in wind energy technologies, however, hold the promise of producing more robust, efficient, reliable, and inexpensive turbines.

One of the major wind technology problems is constraining the operating revolutions per minute (rpm) of wind turbines. As a result of high winds or a loss of generator load, the rotor may rotate in an overspeed condition, possibly causing significant damage to the turbine. Consequently, rotor speed should be controlled so that it is safe. Mechanical brakes are adequate to hold a stopped rotor, but they are usually ineffective at high rotation speeds and tend to be expensive and unreliable. Considering how wind turbines operate, the most direct method of controlling rotor rpm is by reducing the rotor aerodynamic driving forces. This method of limiting turbine speed is often called "aerodynamic braking."

In addition to the potential overspeed problem, dirt, and accumulated insect impacts, and even minor blade damage can result in less than desired power output from turbines. To compensate for these inevitable effects, turbine rotors can be designed for higher than rated power output levels, and small variations in the blade driving forces can be used to modulate or adjust the power to the desired level. As a result, a more consistent power production level can be obtained over time. This method of turbine operation or control is commonly called "power modulation."

Airfoil Trailing-Edge Controls

Airfoil trailing-edge aerodynamic control surfaces offer a direct technique for limiting rotor rotation speeds and performing power modulation. Snyder and Wentz of Wichita State University (WSU) performed extensive research in this area between 1970 and 1980. Indeed, they identified and suggested a number of very promising speed- and power-regulating airfoil designs for wind turbine applications (Snyder, Wentz, and Coa 1985, 1987). Wayman (also of WSU) recently performed a comprehensive investigation on several of these control configurations, including the effect of control pivot location (Wayman 1993).

The airfoil trailing-edge controls are installed over a short span of the turbine blade near the tip, much like an aileron on an aircraft wing. The exact turbine behavior or power output depends on the aerodynamic character of the control device, and on the torque produced by the rest of the turbine blade. Considering only the aerodynamic behavior of the airfoil control, the suction coefficient (C_s) gives a basic measure of the device's ability to influence rotor torque, and thus rotational speed or power output. The suction coefficient is defined as follows

$$C_s = C_l \sin \alpha - C_d \cos \alpha$$

where C_l and C_d are the section lift and drag coefficients, respectively, and α is the airfoil angle of attack.

During normal turbine operation, the suction coefficient is positive, thus promoting rotor rotation and the production of power. A slight change in the suction coefficient effects minor power output changes, (i.e., power modulation), and a large reduction (to a negative value) produces braking torque. To produce large

negative C_S values, one must significantly drop the airfoil lift and increase the drag. This requirement is atypical of most airfoil applications.

Production of very large negative suction coefficient values is extremely important for other reasons besides speed control and power modulation. Other problems relating to control actuation loads, structural complexity, costs, and weight can be minimized by using highly effective airfoil trailing-edge control designs. Unfortunately, identifying controls with extreme negative suction coefficients is very difficult.

The flow field about these special trailing-edge control airfoils can be extremely complex, particularly when control deflections and angles of attack are large. Under such conditions (which are common for wind turbines operating in off-design conditions), extensive regions of separated flow develop. The exact geometry of the main and trailing-edge airfoil elements, along with the Reynolds (R_c) number and angle of attack, can have a significant impact on the flow field behavior. The complicated relationship between these and other factors makes identifying airfoils for aerodynamic braking and power modulation very difficult.

A number of commercial wind turbine manufacturers have shown increasing interest in the use of trailing-edge control devices. However, further improvements are needed to ensure widespread, practical, and reliable application of these controls. Specifically, the aerodynamic effectiveness, hinge-moment behavior, and geometry of current designs must be improved.

Investigation Goals

The National Renewable Energy Laboratory (NREL) recently began a program to identify and develop improved trailing-edge controls for wind turbine power modulation and, more importantly, aerodynamic braking applications. In light of this effort, the goals of their study are as follows:

1. Identify, in cooperation with NREL, its subcontractors, and the wind industry, a number of promising trailing-edge control designs for further study.

2. Conduct wind tunnel tests on the selected controls and compare the basic aerodynamic capabilities of each configuration.

3. Identify, based on the comparative test results, a design for both detailed aerodynamic evaluation and future development.

New Trailing-Edge Control Configurations

A large number of new trailing-edge control configurations were identified jointly by NREL, its subcontractors, and various wind industry representatives. However, because of time and cost limitations, only the five most promising configurations were selected for wind tunnel testing. Final choices were based primarily on their assumed potential for aerodynamic braking applications. Additional details on the various trailing-edge controls are provided by Quandt (1994), who conceived and developed with WSU the various test configurations.

Each of the selected controls was designed to fit an existing wind tunnel model by Northern Power Systems (NPS). The base airfoil shape for this model is approximately that of a NACA (National Advisory Committee for Aeronautics) 64_3-618 section, and all of the controls are assumed to match this shape when undeployed. However, once the control surfaces are actuated, the airfoil geometry changes notably. A basic description and schematic diagram for each of the five selected configurations examined are provided in the following sections (also see Figures 1-5). In all cases, the main or forward element of the model airfoil was of 50% chord length (based on the basic airfoil's chord length of 18 inches).

NACA Double Split-Flap/60 Control

Figure 1 shows a schematic diagram of a control configuration called the NACA Double Split-Flap/60, which was originally designed for aircraft dive brake applications in the 1940s (Toll and Ivey 1945). The trailing-edge portion of the airfoil is assumed to simply split into top and bottom panels that deflect to the desired position. For construction simplicity, a single deflection angle of 60° (relative to the aft part of the basic airfoil chord line) was the only one examined during this investigation.

The upper and lower brakes effectively pivoted on the closed control airfoil surface approximately 53% (based on the basic airfoil chord) aft from the airfoil leading edge. With all of the brake segments installed, the vent area gap is said to equal to 0.0%. However, as shown in Figure 1, there is still an open path for the air to move directly behind the brake surfaces. In some cases, this gap was taped shut.

To offer testing flexibility and to make model construction easier, the brake surfaces were composed of brake segments made from approximately 0.125-inch-thick aluminum plates. Each brake segment was attached to supports that were about 0.50 inch thick and spaced at four even intervals along the height of the model. The length, vent gap size, and position of the brake segments on either the airfoil top or bottom could be varied by dismounting or moving segments as desired. The two innermost (i.e., closest to the airfoil surface) brake segments have lengths of 5.0% each, the next segment has a length of 10%, and the outermost segment has a length of 20% (all based on the basic airfoil chord length), as shown in Figure 1.

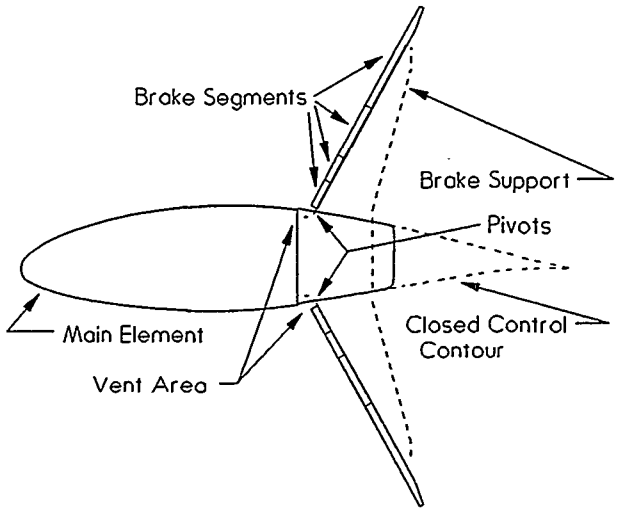

Figure 1. The basic NACA Double Split-Flap/60 control configuration.

NACA Double Split-Flap/112 Control

Figure 2 shows a schematic diagram of a control configuration called the "Clam-Shell," or NACA Double Split-Flap/112 configuration. During operation, a portion of the upper and lower surface is assumed to open outward to a fixed deflection angle of 112° (as measured relative to the aft part of the basic airfoil chord line). As was the case for the NACA Double Split-Flap/60 configuration, each brake surface was made from flat 0.125-inch-thick aluminum plates connected to four 0.50-inch-thick supports mounted on the main element. Unlike the Double Split-Flap/60, the afterbody of this configuration has a solid trailing-edge element. The area between the forebody and afterbody is open, and air was free to move between the upper and lower airfoil surfaces during the tests.

The effective pivot location of each brake surface was located approximately 75% from the airfoil leading edge and 2% above the chord line. The length and location of a complete brake panel could be adjusted depending on the number and mounting location of the brake segments used. Three brake segment lengths were examined. Figure 2 shows the innermost segment with a length of 5% and an outer segment with a length of 10%. During testing these two segments were replaced by a single segment of 20% total length. A 5% vent gap between the trailing-edge surface and the inboard end of each brake panel was used for all configurations.

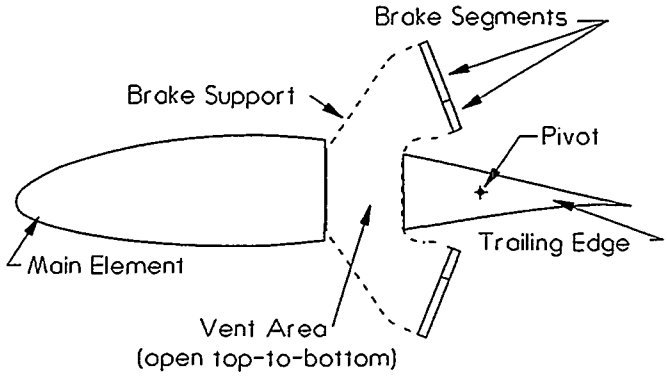

Figure 2. The basic "Clam-Shell" or NACA Double Split-Flap/112 control configuration.

Smooth-Shoulder Control

Figure 3 shows a schematic diagram of the Smooth-Shoulder control configuration. The installed control was capable of deployment at any deflection angle in the negative (i.e., trailing edge up) direction. During actuation, the forward lower edge of the control would ride over a smooth rounded surface or shoulder without venting. The control pivoted about a point located approximately 50% aft of the leading edge and 7% above the chord line, and the shoulder had a radius of approximately 12% (relative to the control pivot point).

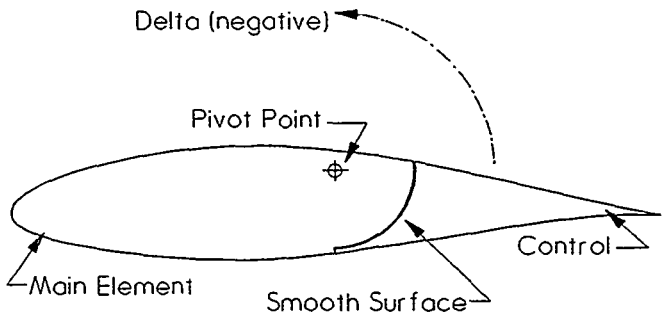

Figure 3. A diagram of the basic Smooth-Shoulder control configuration.

Spoiler-Flap Control

Figure 4 shows a schematic diagram for the Spoiler-Flap (patent pending) control configuration. This particular control is also capable of infinite deflection angles, though only in the positive (i.e., trailing edge down) direction. The control pivot location is approximately 73% from the airfoil leading edge and 1% above the chord line. A small (approximately 1% length) lip extends from the forward upper edge of the control. This lip serves to seal the airfoil upper surface gap prior to control deployment. However, this lip extends up and into the flow above the airfoil once the control starts to deflect. After the control rotates approximately 40°, a relatively unblocked flow between the upper and lower surfaces can take place in the area between the main element and the control leading edge.

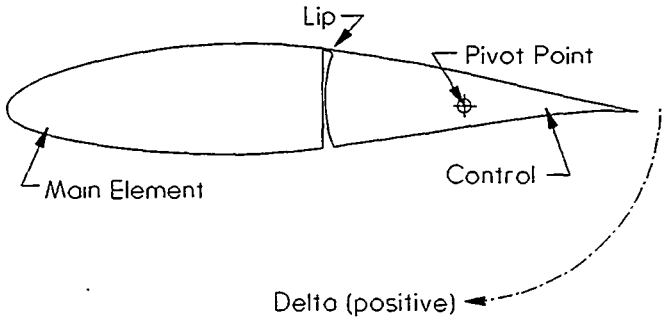

Figure 4. A diagram of the basic Spoiler-Flap (patent pending) control configuration.

Negative-Camber Control

Figure 5 shows a diagram of the Negative-Camber (patent pending) control used in this investigation. The control, which pivots at the same location as the Spoiler-Flap, is capable of deflections in the negative

(i.e., trailing edge up) direction up to 90°. As Figure 5 shows, the lower surface between the main and control elements is open and not smooth prior to deflection of the control.

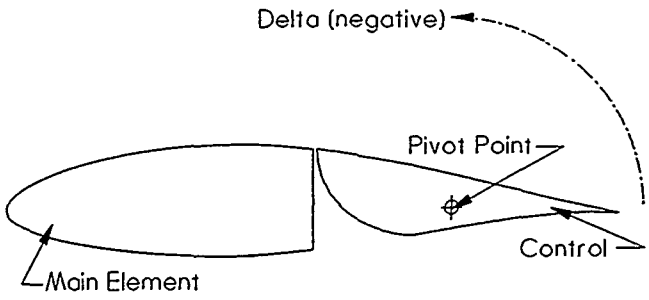

Figure 5. A diagram of the basic Negative-Camber (patent pending) control configuration.

Geometry Modifications: Spoiler Span, Roughness, Stall-Strips, and Vortex Generators

The five configurations discussed above formed the primary group of airfoil shapes that were examined during the wind tunnel tests. However, some simple geometry modifications were made to the NACA Double Split-Flap/60, Spoiler-Flap, and Smooth-Shoulder configurations.

A trailing edge section was added to the NACA Double Split-Flap/60, and the brake panel on the lower surface was removed to produce a simple Airfoil-Spoiler configuration. The span of the upper spoiler panel could be reduced from 100% (i.e., two-dimensional) to 75% and 50% span. These model configurations were examined to identify the approximate impact of partial span controls on aerodynamic performance. Figure 6 shows a diagram of the Airfoil-Spoiler configuration.

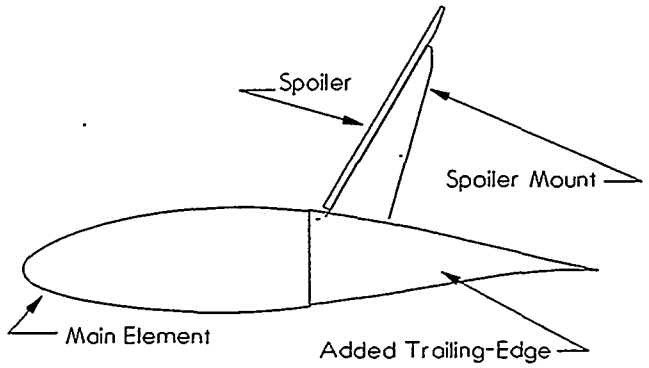

Figure 6. Schematic diagram showing the Airfoil-Spoiler configuration examined, as derived from the NACA Double Split-Flap/60 configuration.

Roughness was applied to the Spoiler-Flap airfoil section in order to identify the aerodynamic performance effect of surface irregularities. Silicon dioxide, of 60-grit size, was applied to the model leading edge using a roughness template supplied by NREL and thin double-stick tape.

A stall-strip and Vortex Generators (VGs) were also fit to the Smooth-Shoulder model in an attempt to identify methods for improving the braking capability for this particular control configuration. Figure 7 shows a diagram of the Smooth-Shoulder model with both the leading-edge stall-strip and the VGs installed. The stall-strip was made from an "L-shaped" aluminum beam (each leg was 2% of the airfoil

chord), and it was mounted (using tape) on the centerline of the model leading edge. VGs were installed alternately at an angle of approximately +/- 15° (from the stream-wise direction), and at a spanwise spacing of 5.5%. Each VG had a trapezoidal planform and a height of approximately 1.4%, a root chord of 5.5%, and a tip chord of 4.2%, all referenced to the airfoil chord.

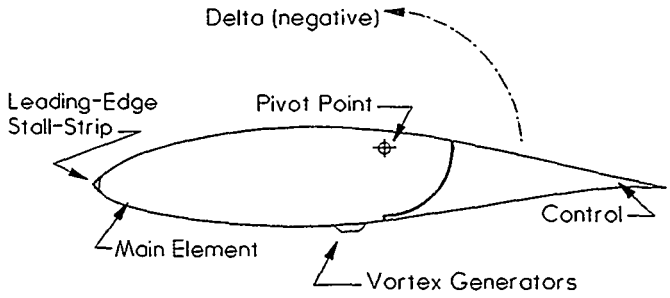

Figure 7. Diagram of the modified Smooth-Shoulder configuration with a leading edge stall strip and VGs installed.

Wind Tunnel Investigation

Each of the configurations described above was evaluated in the WSU Walter H. Beech Memorial 7 X 10 foot low-speed wind tunnel (Johnson 1993), a closed-return design capable of test section dynamic pressures of up to 60 pounds per square foot (psf). The aerodynamic performance of the candidate controls was evaluated in detail during approximately 60 hours of tests. The following sections discuss, in detail, specific aspects related to the design, installation, and testing of the model configurations.

Model Design

NPS supplied the wind tunnel model which was modified in the WSU machine shop to serve as the basic test apparatus. The main element, or forward part, of the basic model, with an approximately a 9-inch chord and 84-inch span, was used during the entire investigation. New or modified parts were installed to the aft half of the model as needed to produce the various test configurations. In addition, end plates and an aerodynamically improved control actuator were incorporated on the original NPS model in order to reduce aerodynamic tare and interference effects.

All of the aerodynamic controls examined, except the NACA Double Split-Flap/60 and Double Split-Flap/112, required control deflections through a range of different angles. An electrically controlled actuator, positioned below the tunnel floor, was used for this purpose. A rotating driveshaft, a control arm, and a control link were the only parts of the actuator mechanism that were exposed to the flow during the tests.

Figures 8a and 8b show an end view of the control deflection actuator system used during the investigation. Mechanism components that are below the tunnel floor are drawn using dashed lines. The control arm and link were approximately 0.50 inches high and 0.75 inches wide. Although thess figures show the Spoiler-Flap configuration, it should be noted that different length links, connecting points, and directions of actuator motion were required for each control evaluated. The basic setup was very similar for all tests, however.

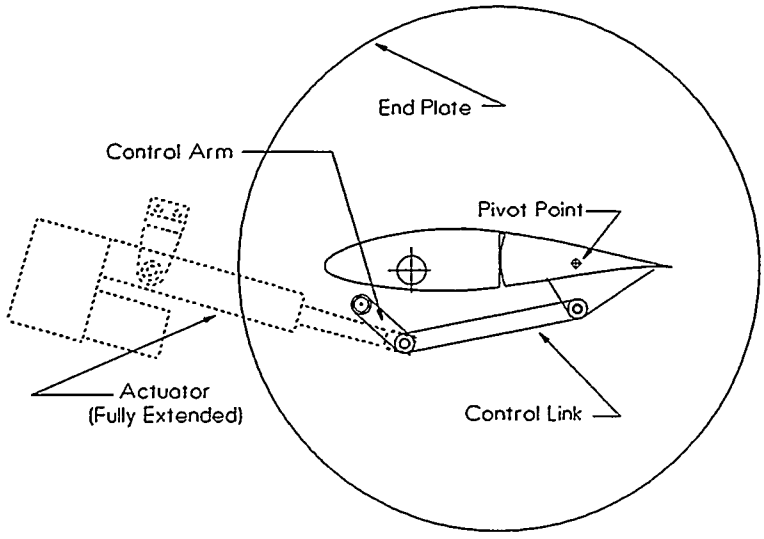

Figure 8a. An end view of the control deflection mechanism, with the control in an un-deflected condition.

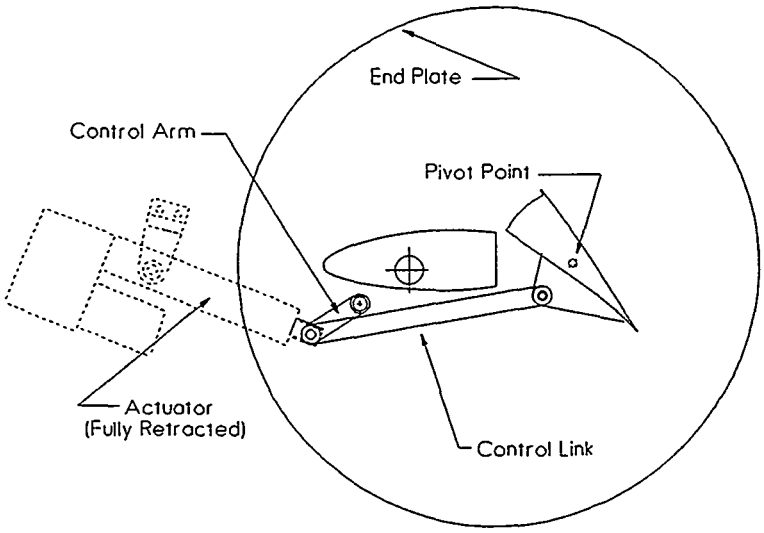

Figure 8b. An end view of the control deflection mechanism, with the control deflected to positive 45°.

Model Installation

The model was mounted in the test section vertically from the tunnel floor to the ceiling, thus forming a two-dimensional installation. Circular end plates, with a diameter of 27 inches, were attached to the model and served to minimize three-dimensional and leakage flow near the tunnel walls. The end plates were approximately 0.187 inches thick and had smoothly rounded edges. Figures 8a and 8b show the relative location and size of the model and end plates.

The model was supported by two wind tunnel balances that together measured the net two-dimensional lift, drag, and quarter-chord pitching moments loads. A photograph of the Spoiler-Flap configuration installed in the WSU wind tunnel test section (with zero control deflection) is shown in Figure 9. A six-component pyramidal-type external balance recorded approximately half of the model lift and drag forces and all of the pitching-moments about the quarter-chord. A specially constructed two-component balance, connected to the top end of the model, measured the remaining model lift and drag. The output from the two balances was combined to determine total model aerodynamic loads. The use of two wind tunnel balances was necessary to ensure that force limits on the pyramidal balance were not exceeded. Balance roll-direction loads would have been larger than allowable if a simple cantilever installation had been used.

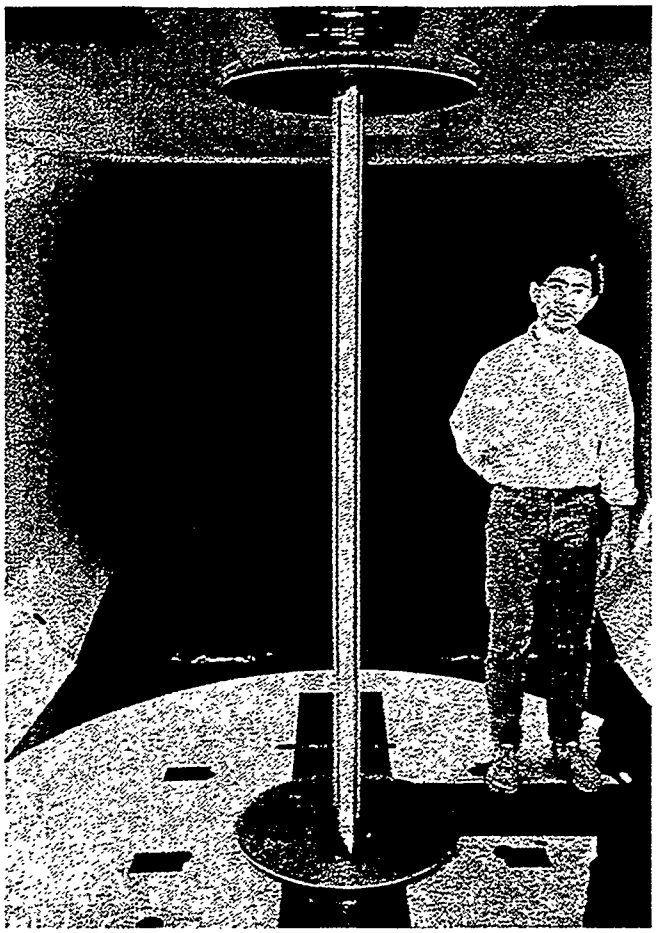

Figure 9. A photograph of the test model installed in the WSU 7 X 10 foot low-speed wind tunnel (showing an aft view of the Spoiler-Flap configuration).

Wake Velocity Surveys

The drag forces measured by the tunnel balances also include aerodynamic loads from the model mounts, end plates, control actuator mechanism, and aerodynamic interferences (from leakage and three-dimensional flow). A means to identify or estimate the aerodynamic drag of these factors, called tares and interferences, was thus needed.

By measuring the wake velocity profile, one can calculate very accurately, via momentum theory, the two-dimensional airfoil section and control drag. (Johnson 1993). Ordinarily this would be the best way to get good aerodynamic drag information on an airfoil, but the technique is very time consuming to complete. Balance drag measurements can be obtained much more quickly. Limited use of the wake survey method does, however, offer a means for defining the tare and interference loads.

For the current investigation, tare and interference were defined as a function of angle of attack, for only one model configuration. The Negative-Camber control model geometry was used because it seemed to represent, in an average sense, many of the candidate configurations. It was then assumed that this tare and interference data could be used to correct the balance-measured drag data for all other configurations examined. This approach offers a time-efficient means to obtain quality airfoil and control drag data.

The following equations illustrate mathematically how the wind tunnel model tare and interference drag are defined. For each angle of attack, the balance measures a drag value. This balance-measured drag is composed of many parts, as is shown in the following equation:

$$Drag_{Balance\ Measured} = (Drag_{Two\text{-}Dimensional\ Airfoil\ \&\ Control}) + (Drag_{End\ Plates} + Drag_{Actuator} + Drag_{Mounting\ Fixture} + Drag_{Aerodynamic\ Interference})$$

The wake survey measurements and momentum equation integration yield the following:

$$Drag_{Wake\ Momentum\ Calculations} = (Drag_{Two\text{-}Dimensional\ Airfoil\ \&\ Control})$$

The model tare and interference drag is composed of all drag loads other than that of the two-dimensional airfoil and control, or as is now given:

$$Drag_{Tare\ and\ Interference} = (Drag_{End\ Plates} + Drag_{Actuator} + Drag_{Mounting\ Fixture} + Drag_{Aerodynamic\ Interference})$$

The tare and interference drag function can thus be defined by simply taking the difference between the balance-measured and wake momentum calculated values at each angle of attack, as the next equation shows.

$$Drag_{Tare\ and\ Interference} = (Drag_{Balance\ Measured}) - (Drag_{Wake\ Momentum\ Calculations})$$

Static-Pressure Belts

Surface static-pressure distributions were obtained for the Negative-Camber and Spoiler-Flap configurations by using pressure belts. This particular measurement technique is widely used in the aircraft industry and offers the opportunity to obtain static-pressure distribution data on a model or surface that was not initially outfitted with internal pressure taps. Results from these measurements provide detailed information on the airfoil section load distributions and, after integration, on the control actuation hinge-moment levels.

Pressure belts are constructed by using commercially available tygon rubber-tubing belts (commonly called "Strip-O-Tubes"). Normally these belts are used simply to connect pressure ports to a transducer system and because they are straps instead of individual tubes, they are easier to work. However, for surface static-pressure measurement applications, they are modified and used differently. Specifically, one end of the belt has air-tight plugs inserted into each individual tube. An approximately 0.005-inch-diameter hole is drilled perpendicular to the flat side of the belt surface in each tube at a desired location. The other end of the belt is then routed to pressure transducers, typically using more tubing belts in the traditional manner. As a result, each individual belt can measure a static-pressure at ten points along its length. As many belts as are needed are then simply mounted, via double-stick tape, to the model surface.

Three belts, each approximately 1.5 inch wide by 0.125 inch thick, were mounted on the main and control surfaces of the test configurations. A total of 60 static-pressures were measured, 15 on each element's upper and lower surfaces. Figure 10a shows a simplified diagram illustrating the pressure belt installation on the model, and Figure 10b shows a photograph of the belts installed in the Negative-Camber model configuration. The belts were mounted about the model mid-span, and the pressure transducer modules were mounted outside the tunnel test section. As was mentioned previously, additional belts were used to connect the pressure-measuring belts to the pressure transducers. In order to minimize aerodynamic interference, these connecting tubes were taped to the aft side of the main element and to the lower surface trailing-edge side of the control element.

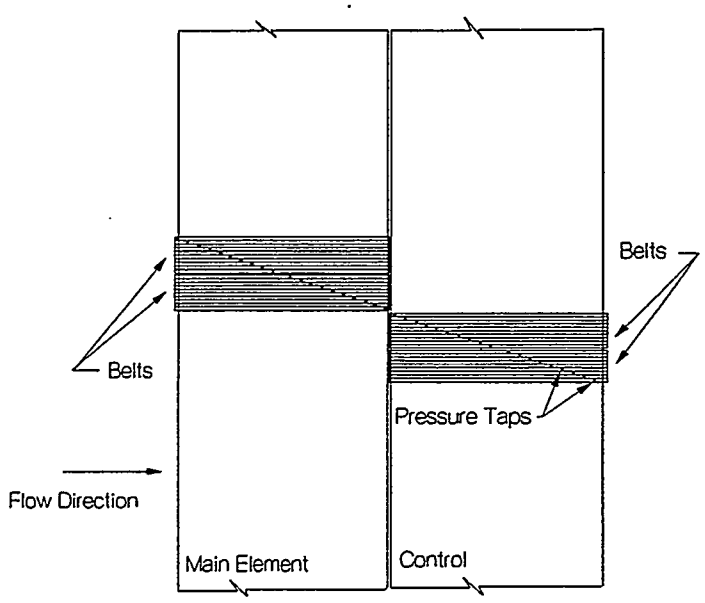

Figure 10a. A simplified diagram showing pressure belts installed on a portion of the wind tunnel model (drawing not to scale).

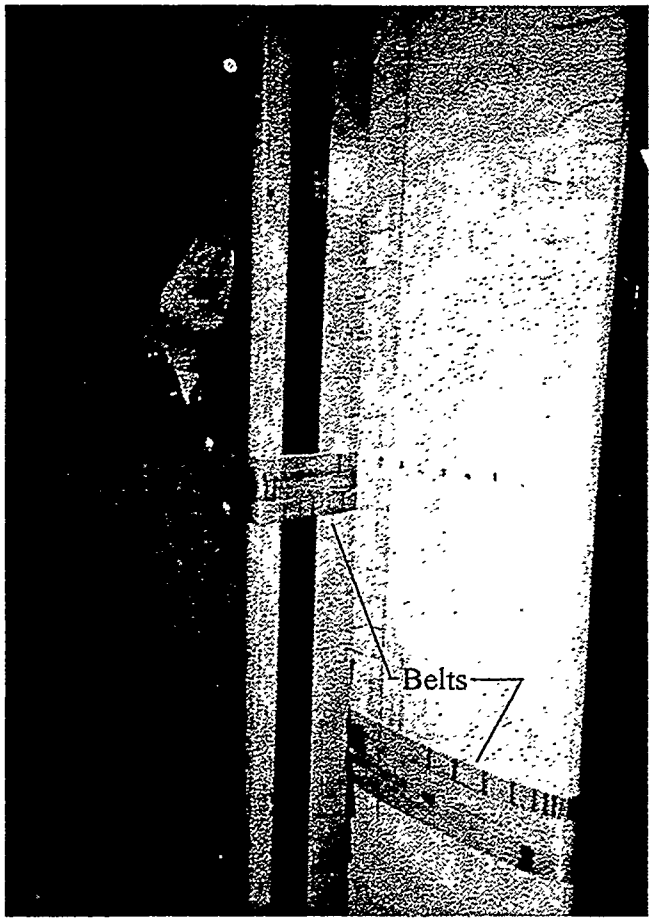

Figure 10b. A photograph showing the pressure belts installed on the Negative-Camber configuration, with the control surface deflected about 45°.

Wind Tunnel Data Acquisition

Data from the various measurement sensors used during the tests were acquired and conditioned as necessary by the wind tunnel data acquisition system. The WSU facility uses an HP-9000 series workstation computer to control and gather test results. This computer is connected to a stand-alone unit, an HP-3852, that provides signal conditioning for various types of measurement instruments and a buffer interface with the host computer. Appropriate data reduction methods are applied to the measurements as needed, and the resulting data are presented in a real-time fashion, as well as in hard-copy or software formats (Johnson 1993).

Model loads, model angle of attack, tunnel dynamic pressure, and test section temperature are continuously monitored and recorded in order to allow accurate measurement of a model's aerodynamic character. Static-pressure distributions and wake-velocity values, as measured by the surface-mounted belts and a traversing 5-Hole probe, respectively, were acquired by a Pressure Systems Incorporated (PSI) pressure measurement system. This system uses solid-state, high-speed scanning pressure transducer modules and communicates directly with the tunnel workstation computer.

A mechanical traversing mechanism was used to move the 5-Hole probe though the model wake. Figure 10c shows a photograph of the apparatus installed in the wind tunnel test section. The traversing device was fitted with an accurate position encoder that was read by the tunnel computer, and the output from the 5-Hole probe was gathered via the pressure system and used to calculate flow direction, speed, and dynamic and static pressures. The measured velocity and position data were then integrated using the momentum equation to define local two-dimensional section drag values (Rae and Pope 1984). These data were then used to define the general tare and interference drag function.

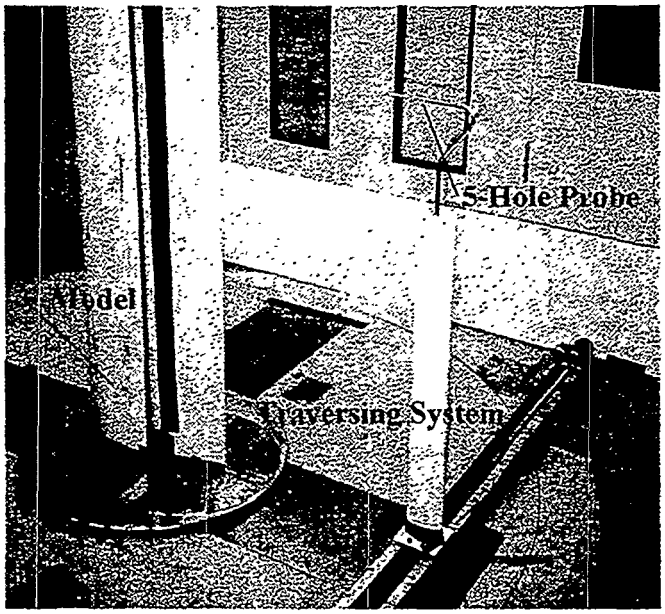

Figure 10c. A photograph showing the wake-traversing mechanism and 5-Hole probe installed in the test section, downstream of the wind tunnel model.

Wind Tunnel Blockage and Flow Corrections

Lift, drag, and pitching-moment data measured directly by the tunnel balances were corrected to account for effects related to testing in the unique environment of a wind tunnel. Standard two-dimensional methods, as presented in Rae and Pope, were used to correct the test data for the influence of flow blockage

(solid and wake), flow angularity, streamline curvature, and buoyancy (Rae and Pope 1984). As has been discussed, model tare and interference drag effects were corrected via the wake-velocity momentum drag calculations.

Test Matrix

Table 1 summarizes the test matrix used during the investigation. As can be seen, a wide range of aerodynamic measurements for more than 200 separate runs was obtained. Basic two-dimensional force and moment data were recorded for each test configuration over an angle-of-attack range between -6° and + 90°, and for control deflections (where applicable) from -6° to +90°. In addition, surface static-pressure measurements and wake surveys were also performed. Tunnel operating dynamic pressures were set as high as feasible (about 15 psf, or 80 mph) to provide the largest Reynolds number data possible (~1,000,000 at the highest speed, based on full chord).

Interestingly, model buffet levels limited wind tunnel test speeds more than any other factor. Tunnel balance load limits were rarely approached. Typically, the models remained stable and steady as angle of attack increased until about 25°, at which time buffet would start. As angle of attack or control deflection increased, the tunnel operator was forced to reduce the dynamic pressure (or wind speed). Under the worst conditions, the tunnel dynamic pressure would be lowered to a value of 3.0 or 5.0 psf by the time tests reached 90° angle of attack.

Table 1. Wind tunnel test matrix summary.

Basic Configuration	Subconfiguration or Comments	Control Deflections (degrees)	Test Data Obtained
NACA Double Split Flap/60	0/40, 5/35, 10/30 & 20/20*	Fixed at 60	Forces & Moments
	Top 4.4/20, Bottom 4.4/20*	Fixed at 60	Forces & Moments
	Top 4.4/20, Bottom 8.9/20*	Fixed at 60	Forces & Moments
	Top 4.4/20, Bottom 14.4/20*	Fixed at 60	Forces & Moments
	Top 0.0/20, Bottom 14.4/20*	Fixed at 60	Forces & Moments
	Top 8.9/20, Bottom 14.4/20*	Fixed at 60	Forces & Moments
	Top 14.4/20, Bottom 14.4/20*	Fixed at 60	Forces & Moments
NACA "Clam-Shell" or Double Split-Flap/112	5/15*	Fixed at 112	Forces & Moments
	Top 5/20 & Bottom 5/15*	Fixed at 112	Forces & Moments
	Top 5/20 & Bottom 5/20*	Fixed at 112	Forces & Moments
	Top 5/15 & Bottom 5/20*	Fixed at 112	Forces & Moments
Smooth-Shoulder	(Basic Model)	0, -10, -30, -60 & -90	Forces & Moments
	Stall Strip	0, -10, -30, -60 & -90	Forces & Moments
	Vortex Generators	0, -10, -30, & -45	Forces & Moments
Spoiler-Flap	(Basic Model)	0, +10, +30, +60 & +90	Forces & Moments
	Roughness	0, +30, +45, +60 & +90	Forces & Moments
	Pressure Belts	+45, +60 & +90	Pressure Distributions
Negative-Camber	(Basic Model)	0, -10, -30, -60 & -90	Forces & Moments
	Wake Surveys (for 0, 2.5, 5.0, 7.5, 10.0, 12.5, & 15.0 degrees angle of attack)	0	Wake Velocities
	Pressure Belts	-40, -45, -60 & -90	Pressure Distributions
Airfoil-Spoiler	Full Span Spoiler, 0/40*	60	Forces & Moments
	3/4 Span Spoiler, 0/40*	60	Forces & Moments
	1/2 Span Spoiler, 0/40*	60	Forces & Moments

* *Number-slash pairs indicate percent chord gap and control length used (i.e., 5/35 means a 5% gap and a 35% control length configuration).*

Aerodynamic Coefficient Results and Discussion

The following sections describe the aerodynamic results obtained for each configuration during the wind tunnel testing. A summary of the lift, drag, and suction coefficient performance of each airfoil configuration is provided first, followed by a comparison between each configuration. The suction coefficient behavior, as a function of angle of attack, will be of primary interest because it is the magnitude and sign of this term that helps to define a given control's potential for turbine speed control and, specifically, braking.

It is important to note that the drag and suction coefficients presented in the following sections have not been corrected for tare and interference effects. The impact of the tare and interference drag on the presented aerodynamic coefficients will be discussed more fully in a later section.

NACA Double Split-Flap/60 Control

Figures 11a, 11b, and 11c show the suction, lift, and drag coefficient behaviors, respectively, of the symmetrical NACA Double Split-Flap/60 configurations as measured during the wind tunnel tests. Four separate curves are shown in these figures, each representing different gap and control length combinations. In this case, the gap and control lengths were varied symmetrically top and bottom. Other asymmetric combinations will be presented and discussed shortly. The plot symbol key describes the specific control subconfiguration studied, using the same syntax as was used to describe the test matrix (see Table 1). To review, the number-slash pairs indicate the percent chord gap and control length used (i.e., 5/35 means a 5% gap and a 35% control length configuration).

As Figure 11a shows, the C_S curve is negative for all configurations and examined angles of attack. This result, as has been mentioned previously, is a desirable behavior for turbine braking applications. However, all of the configurations have peaks, or their least negative suction coefficient values, at approximately 20 ° to 25 ° angle of attack. The impact of control gap and length changes, from the zero gap and 40% length case, is most pronounced at the lowest and highest angles-of-attack. Interestingly, very little effect is noted over 25 ° to 30 °. For the conditions examined, a zero gap and maximum length control appears to offer the best performance compromise over the full angle-of-attack range.

Figures 11b and 11c show the lift and drag coefficients that accompany the suction coefficients presented in Figure 11a. As can be seen, when control gap is increased and control length is reduced, airfoil lift is most affected around stall and at the highest angles of attack. Correspondingly, the drag is changed notably over all angles, but especially for lower ($< 20^{\circ}$) angles of attack.

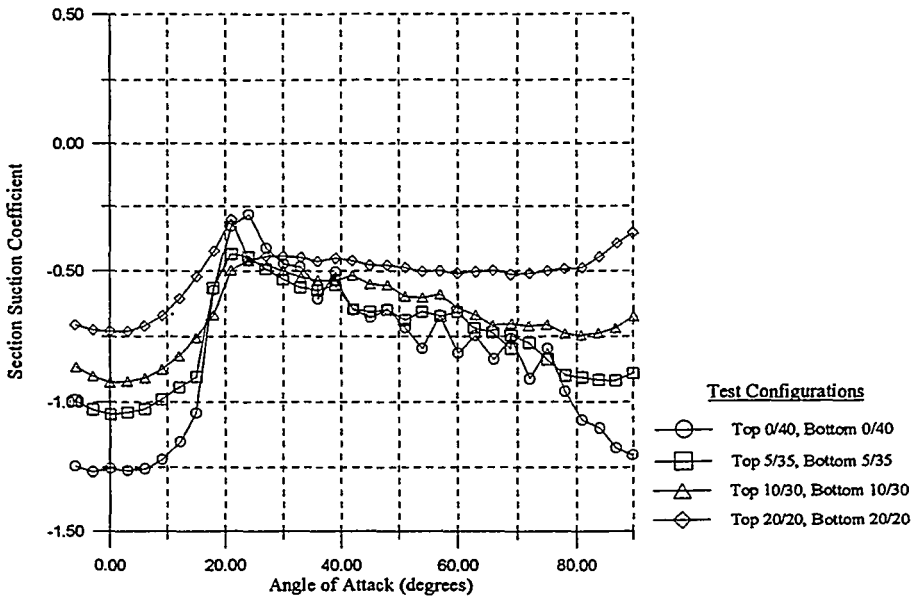

Figure 11a. Suction coefficient behavior for the symmetrical NACA Double Split-Flap/60 configurations.*

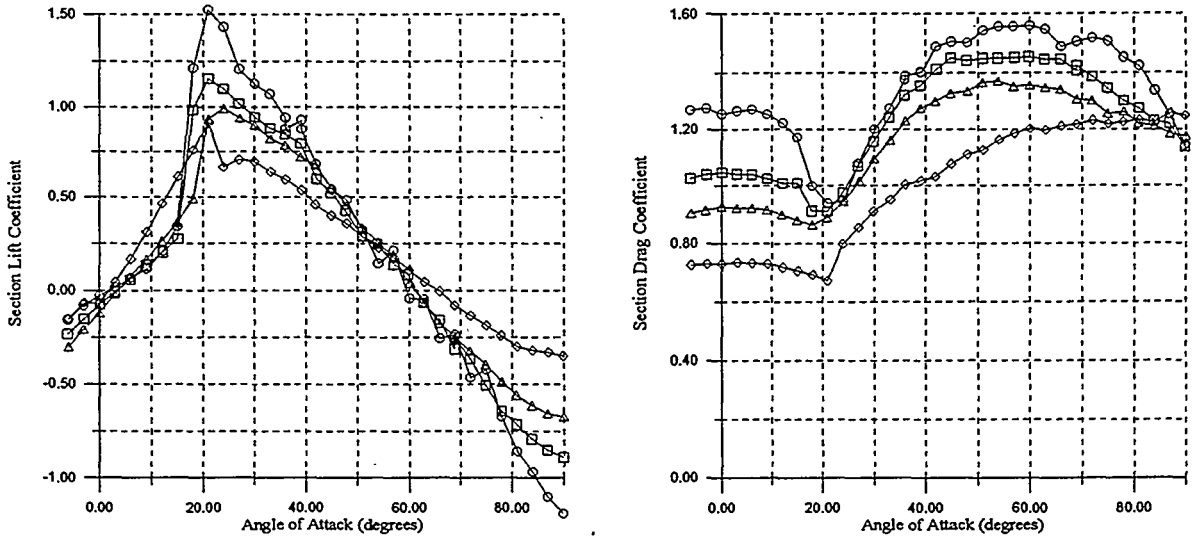

Figures 11b and 11c. Lift and drag coefficient behavior for the symmetrical NACA Double Split-Flap/60 configurations.

* *The number-slash pairs indicate percent chord gap and control length used (i.e., 5/35 means a 5% gap and a 35% control length configuration).*

Figures 12a, 12b, and 12c show the aerodynamic impact of varying the gap on only the bottom surface of the NACA Double Split-Flap/60 airfoil configuration. For each of these cases, the length of both the upper and lower brake panels remains constant and only the bottom gap is varied. Interestingly, only a minor impact on the three aerodynamic coefficients is observed over the full angle-of-attack range as a result of increasing the bottom-surface gap distance.

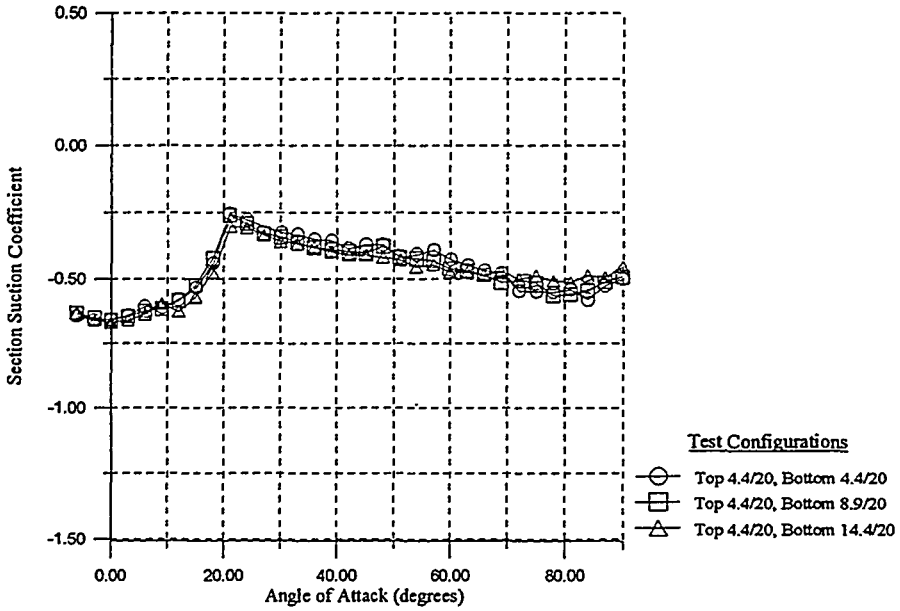

Figure 12a. Suction coefficient for NACA Double Split-Flap/60 configurations with different lower surface gaps.*

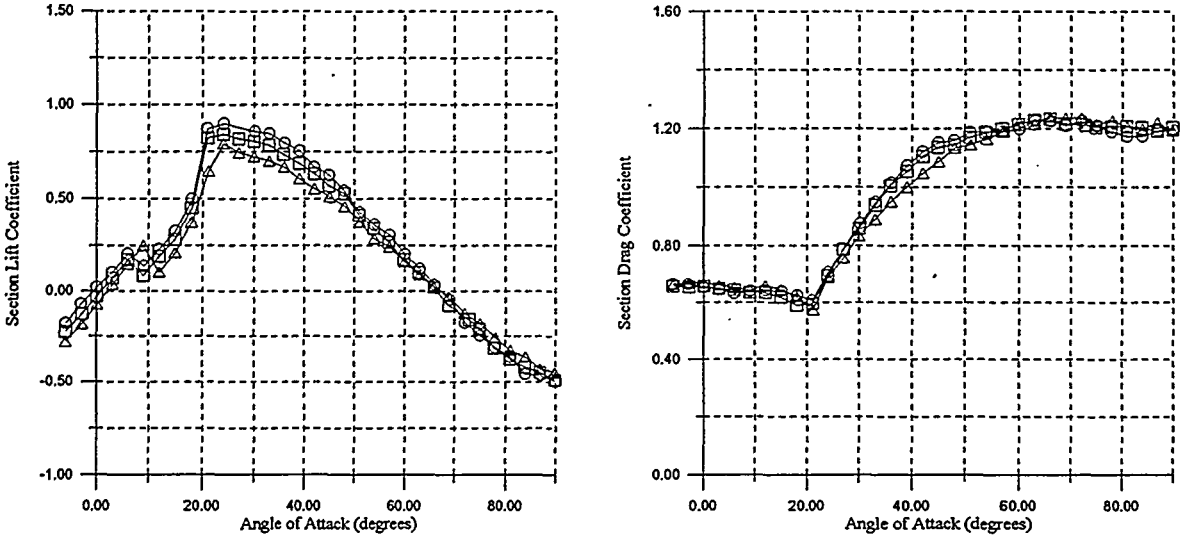

Figures 12b and 12c. Lift and drag coefficient behavior for NACA Double Split-Flap/60 configurations with different lower surface gaps.

** The number-slash pairs indicate percent chord gap and control length used (i.e., 5/35 means a 5% gap and a 35% control length configuration).*

Figures 13a, 13b, and 13c show the effect of changing the gap on only the upper surface brake panel. As was noted for the previous case, only minor differences are produced. The extent of differences is most apparent between 20 ° and 30 ° angle of attack, where the suction coefficient drops slightly.

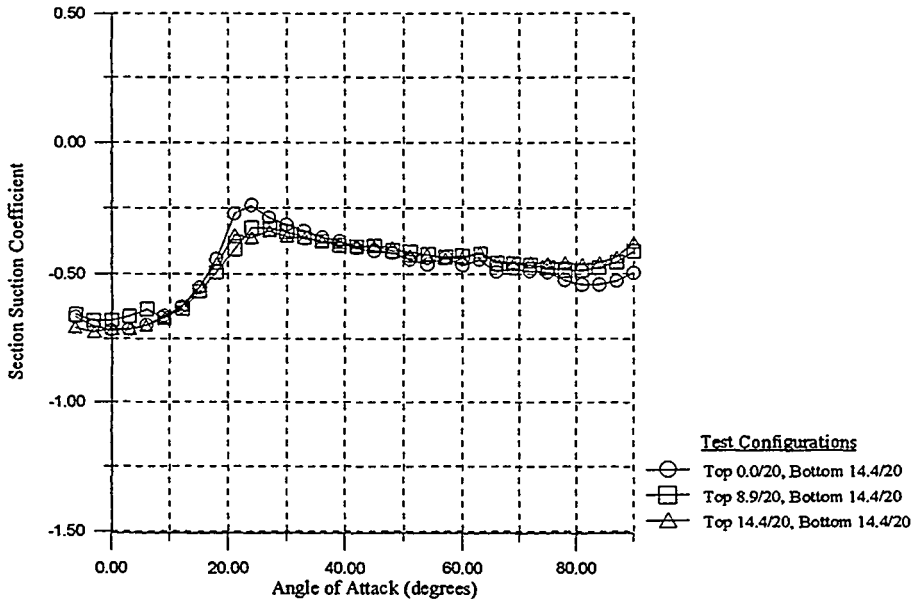

Figure 13a. Suction coefficient for NACA Double Split-Flap/60 configurations with different upper surface gaps.

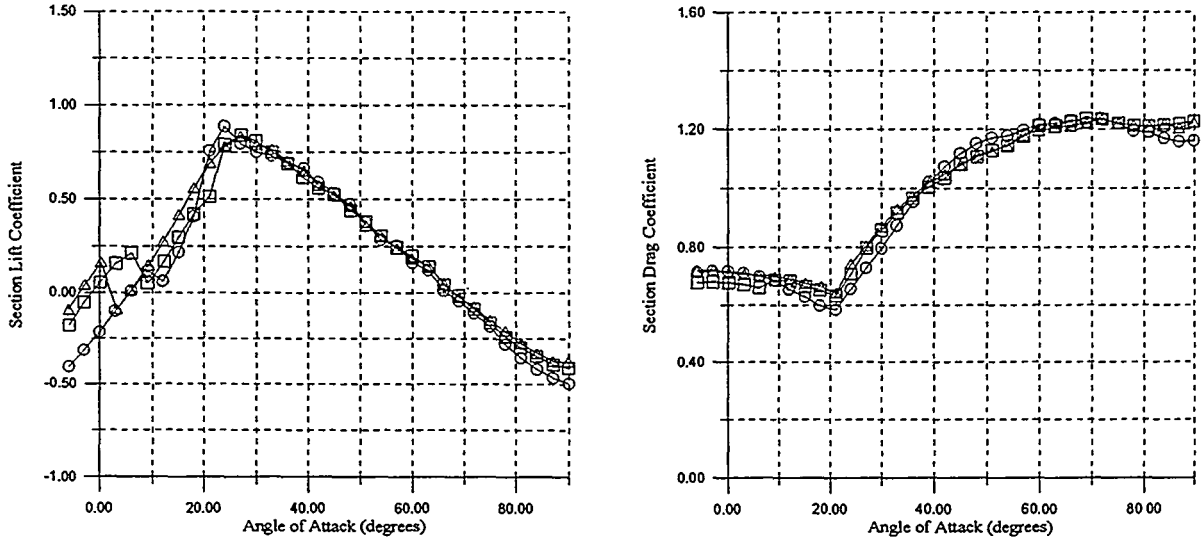

Figures 13b and 13c. Lift and drag coefficient behavior for NACA Double Split-Flap/60 configurations with different upper surface gaps.

** The number-slash pairs indicate percent chord gap and control length used (i.e., 5/35 means a 5% gap and a 35% control length configuration).*

NACA Double Split-Flap/112 Brake Control

Figures 14a, 14b, and 14c show aerodynamic coefficient data for the "Clam-Shell" or Double Split-Flap/112 configuration. Again, the plot symbol key defines the various subconfigurations examined. (The exact subconfiguration is described using the established gap and control length syntax.) As can be seen, two of the permutations used a symmetrical top and bottom chord length combination.

In general terms, as Figure 14a illustrates, all subconfigurations produced negative suction coefficients. However, the coefficients moved slowly in the positive direction as the angle of attack increased. Variations in the control length and asymmetry (top and bottom) were observed to produce the largest changes in the suction coefficient behavior at angles of attack below about 50°. The best control subconfiguration had both upper and lower surface brakes of 20% length. When control lengths were asymmetrical, it appeared more important to have a longer control on the lower surface of the configuration, because this would likely produce better mid-to-high (20° -60°) angle-of-attack braking performance. Figures 14b and 14c show the corresponding lift and drag coefficients.

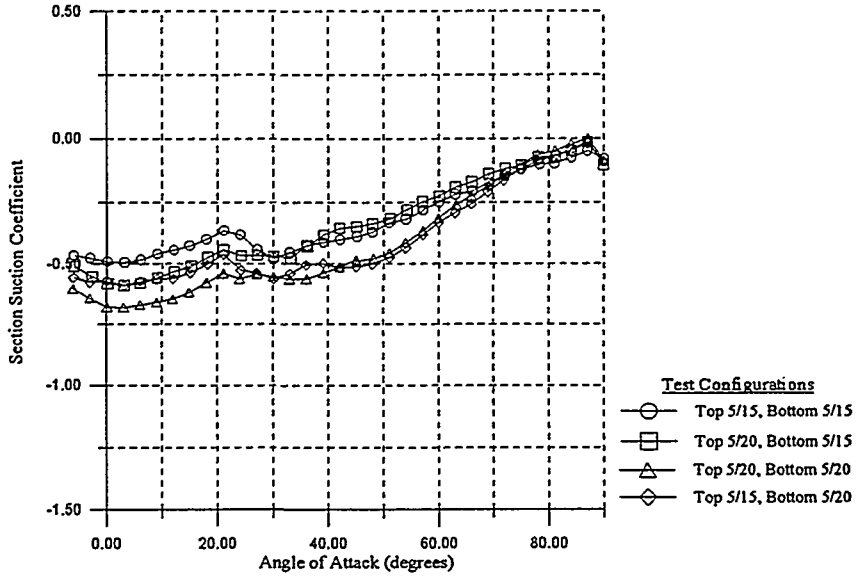

Figure 14a. Suction coefficient behavior for NACA Double Split-Flap/112 (Clam-Shell) brake configurations.*

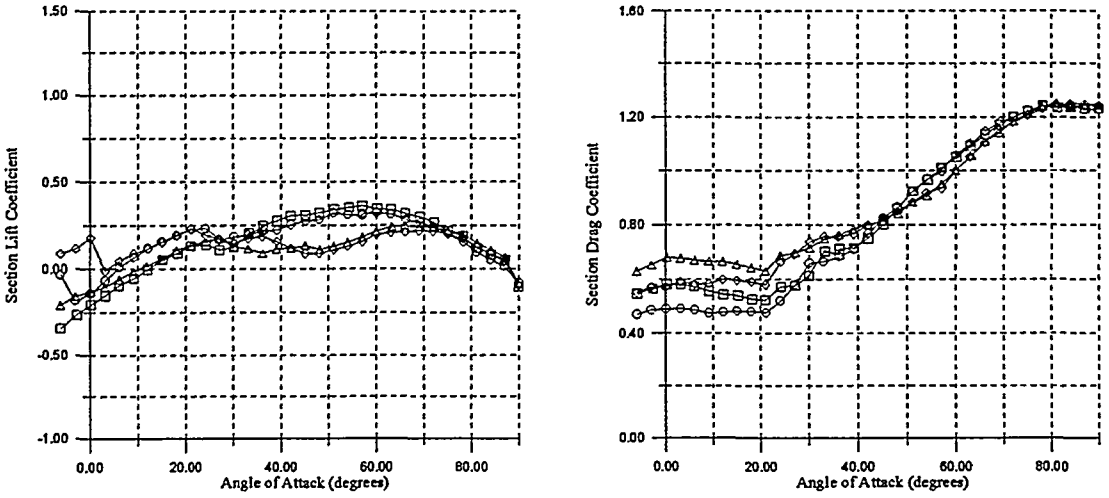

Figures 14b and 14c. Lift and drag coefficient behavior for NACA Double Split-Flap/112 (Clam-Shell) configurations.

Smooth-Shoulder Control

Figures 15a, 15b, and 15c present aerodynamic data for the Smooth-Shoulder configuration as a function of five different control deflection angles. None of the control deflections examined produced negative suction coefficients over the entire angle-of-attack range. However, delta values of -60° and -90° produced very significant reductions in C_S for angles of attack less than 20° and 30°, respectively. Beyond approximately 45° angle of attack, at least -60° delta appears necessary to ensure that negative suction occurs. For a control deflection of -90°, wind tunnel tests had to be ended at an angle of attack of 75° because of severe model buffeting, even at extremely low tunnel operating speeds. Interestingly, this is the only trailing-edge control configuration that experienced this severe of a problem.

The lift coefficient curves shown in Figure 15b illustrate that increasing control deflection angles had a "de-cambering" effect, because the section angle-of-zero-lift became more positive and the stall lift coefficient dropped in magnitude. For deflections of 90°, the control produced very negative lift coefficients for all angles of attack less than 30°. Figure 15c illustrates that, for angles-of-attack lower than approximately 15°, the drag coefficient increased as control deflection increased. The exact impact of control deflection on the drag was more difficult to identify over the 15° to 40° angle of attack range, but above 40°, control deflections reduced the drag coefficient magnitude.

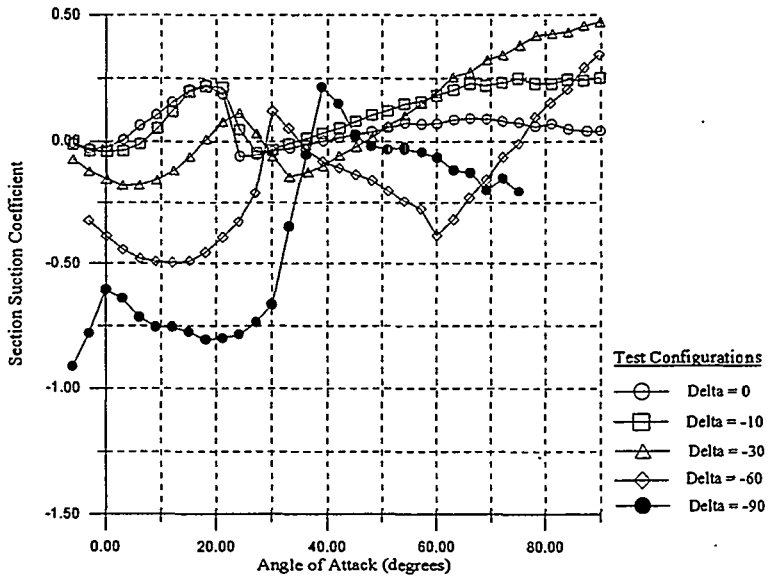

Figure 15a. Suction coefficient summary for the Smooth-Shoulder configuration.

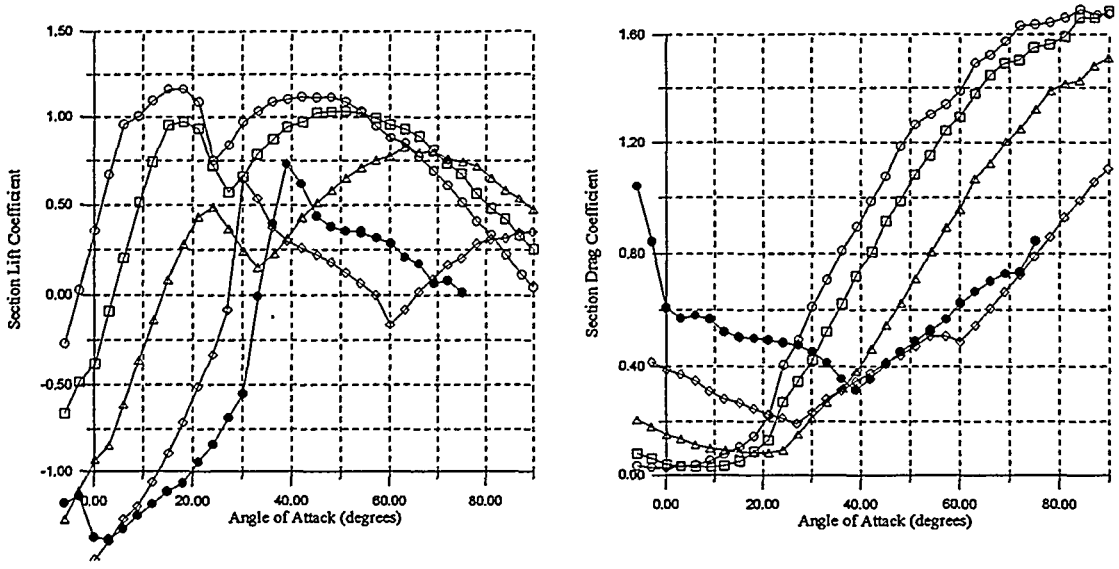

Figures 15b and 15c. Lift and drag coefficient behavior for the Smooth-Shoulder configuration.

Figures 16a and 16b identify the impact of a leading-edge stall-strip and Vortex Generators on the Smooth-Shoulder control's aerodynamic performance for two control deflections. It was hoped that the use of these devices would enhance the performance of this particular configuration. Unfortunately, as can be seen, the effect of these modifications on the suction coefficient curve is minimal. Because of testing time limitations, only one stall-strip mounting location and VG configuration could be examined. It is conceivable that the specific devices used are not optimum.

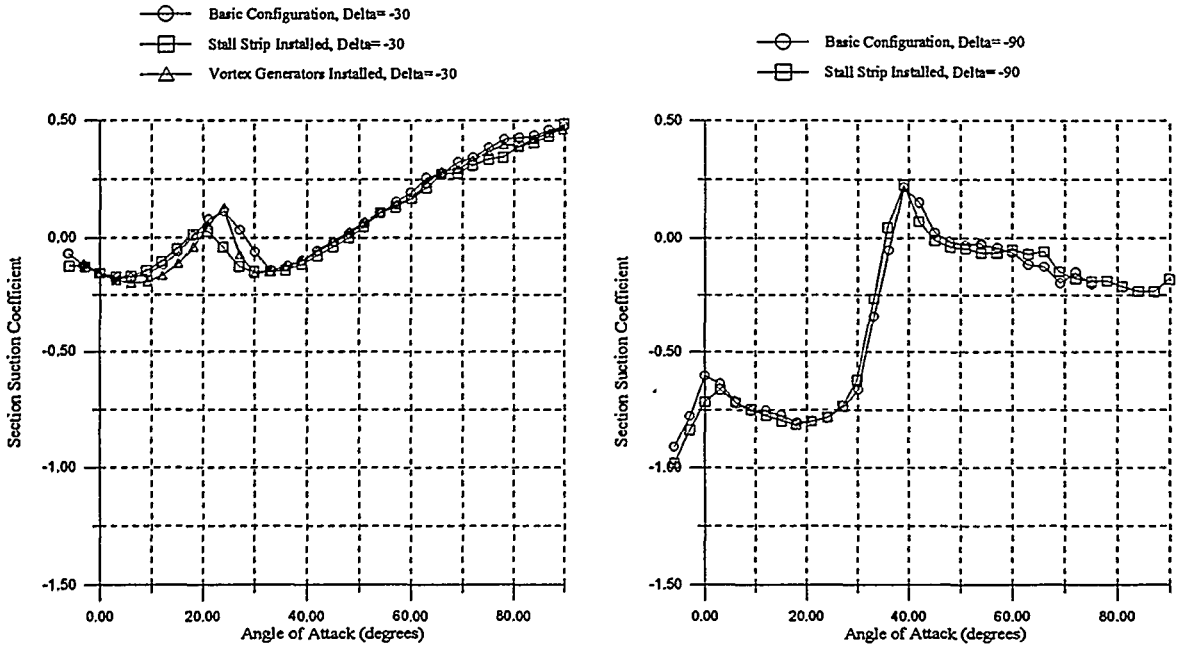

Figures 16a and 16b. Impact of leading-edge stall-strip and Vortex Generators on the Smooth-Shoulder suction coefficient behavior.

Spoiler-Flap Control

Figures 17a, 17b, and 17c show, the suction, lift, and drag coefficient curves, respectively, obtained for the Spoiler-Flap configuration as a function of various control deflection angles. As can be seen in Figure 17a, the suction coefficient becomes negative for all angles of attack once the control device is deflected beyond approximately +30°. For control deflection angles of +60° and +90°, the suction coefficient curve is nearly constant and very negative over the entire testing range.

Lift measurements shown in Figure 17b indicate that those control deflections greater than +60° cause a substantial loss in lift for all examined conditions, especially beyond 20° angle of attack. As can be observed, for a control deflection of +90°, the lift curve slope is approximately zero or negative, and the maximum lift coefficient is about 0.35 over the entire test range. Figure 17c indicates that the drag increases notably with increasing control deflections for angles of attack less than about 30°, after which the drag is left nearly unchanged or even reduced.

The exact impact of the lip, located on the upper leading-edge of the Spoiler-Flap control, is hard to identify based on the current results. However, the lip may cause notable flow separation as the control begins to deflect, thus spoiling the lift and increasing the drag significantly.

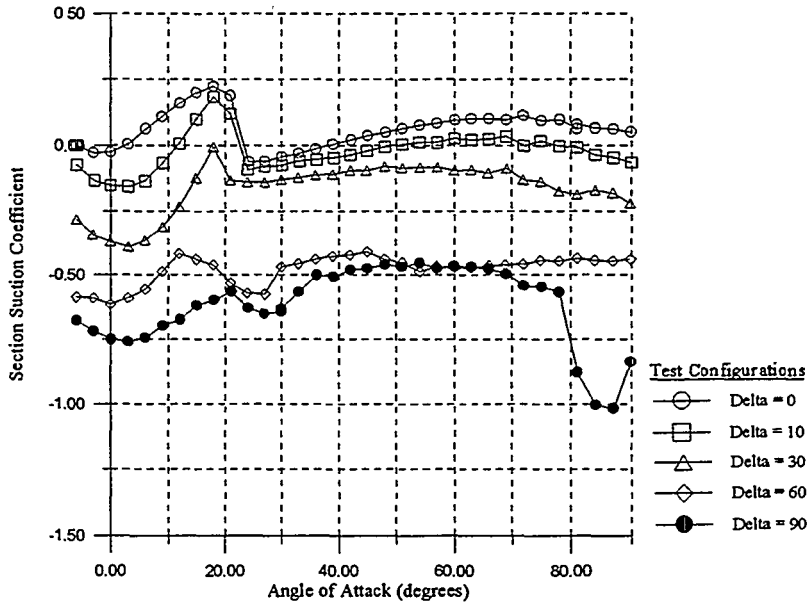

Figure 17a. Suction coefficient summary for the Spoiler-Flap configuration.

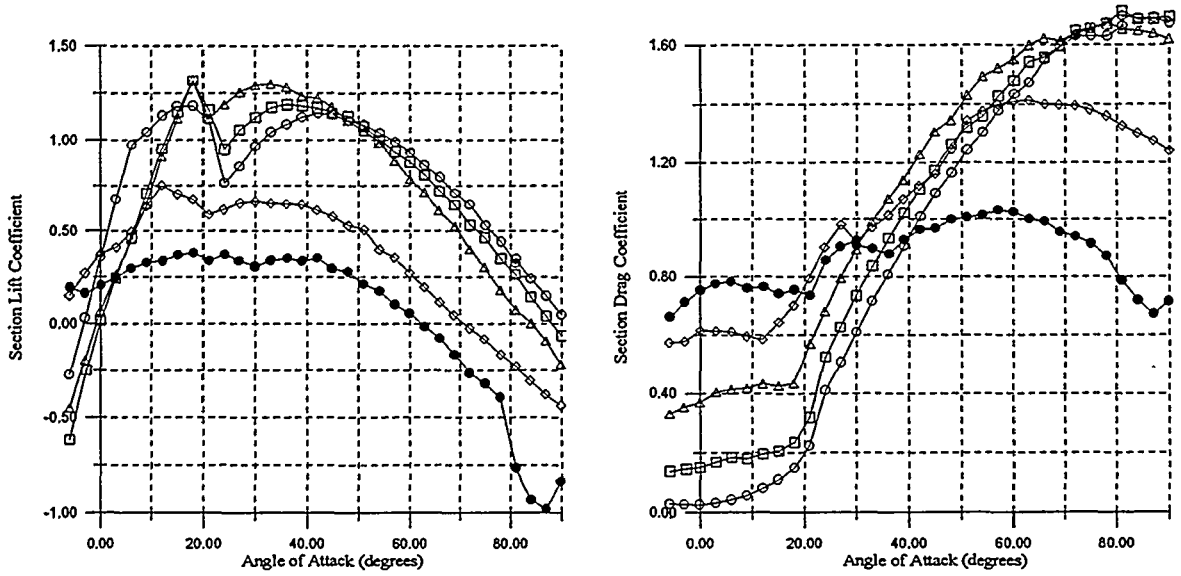

Figures 17b and 17c. Lift and drag coefficient behavior for the Spoiler-Flap configuration.

The effect of leading-edge surface roughness on the Spoiler-Flap configuration performance is shown in Figure 18 at four separate control deflections. As can be observed, roughness (dashed lines) appears to have only a minimal impact on the suction coefficient behavior of the control.

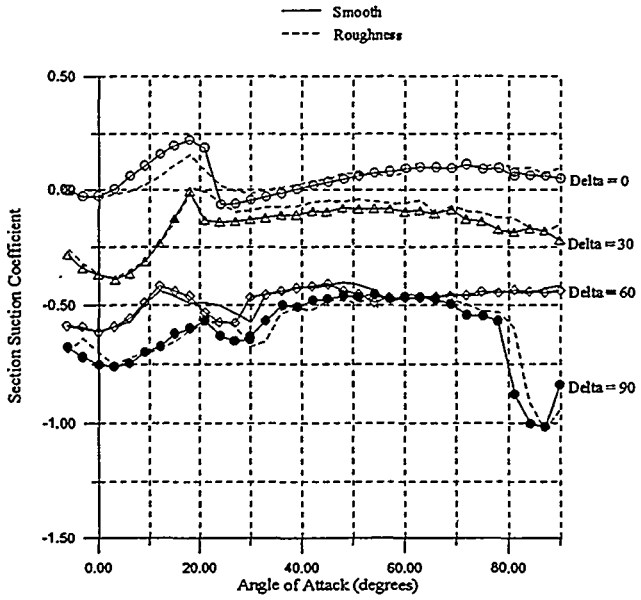

Figure 18. Impact of surface roughness on the Spoiler-Flap suction coefficient behavior.

Negative-Camber Control

Figure 19a describes the suction coefficient variation of the Negative-Camber control configuration as a function of control deflection and angle of attack. Only the -60° and -90° control positions offered a completely negative suction coefficient variation over the test range, and the -90° deflection offered the best overall performance. The general behavior of the curve was nearly constant, as desired, except within the 30° to 60° angle of attack range, where a peak in suction was noted. This peak, however, is still negative in magnitude.

Figure 19b shows that once control deflections decreased below -60°, a notable drop in lift occurred over the entire range. As control deflections became more negative, drag increased for angles of attack less than about 30° and decreased for angles of attack greater than 30°. This particular result is illustrated in Figure 19c.

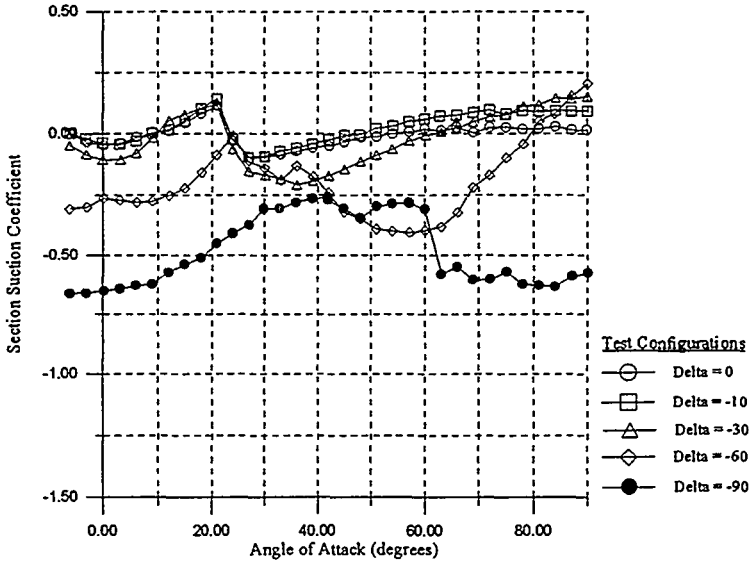

Figure 19a. Suction coefficient summary for the Negative-Camber control configuration.

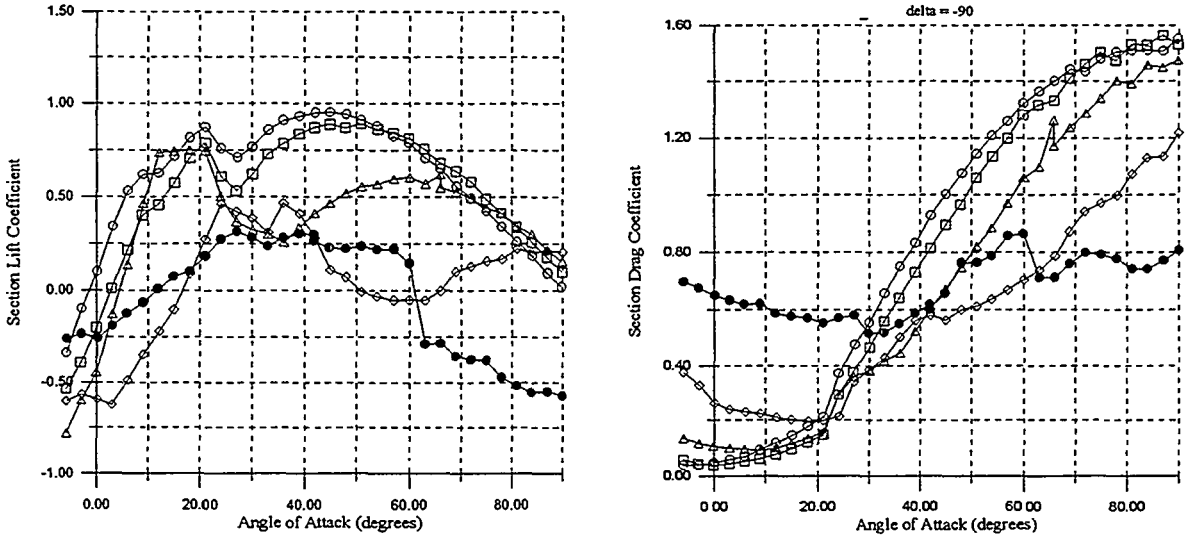

Figures 19b and 19c. Lift and drag coefficient behavior for the Negative-Camber control configuration.

Variable-Span Spoiler

A quick indication of the aerodynamic impact of control span on aerodynamic performance is provided for the Airfoil-Spoiler configuration in Figures 20a, 20b, and 20c. The coefficients in these plots are based on the same reference values used for the other two-dimensional configurations examined. The data is simply presented at this point; a more detailed analysis of this data will be provided in the future.

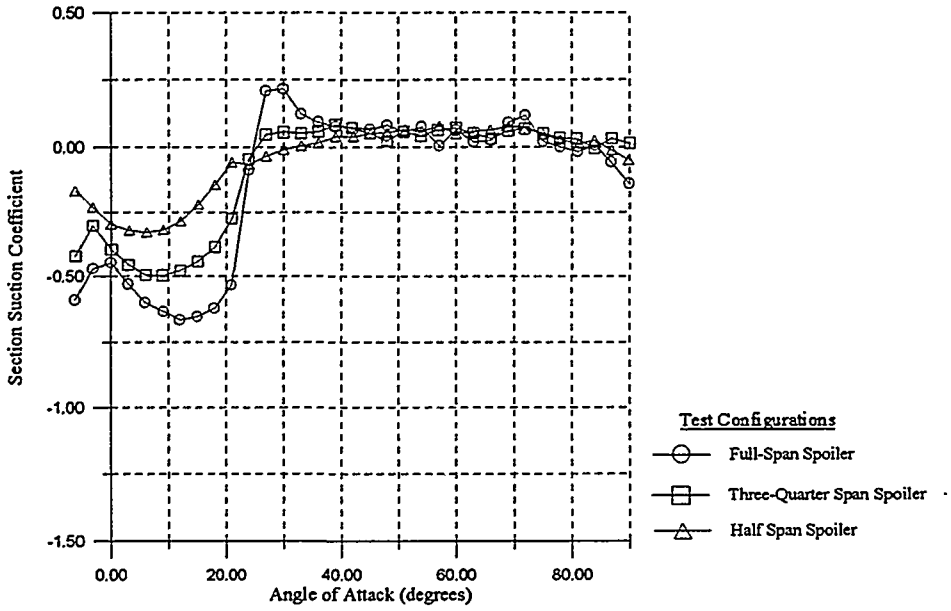

Figure 20a. Suction coefficient summary for the Airfoil-Spoiler configuration.

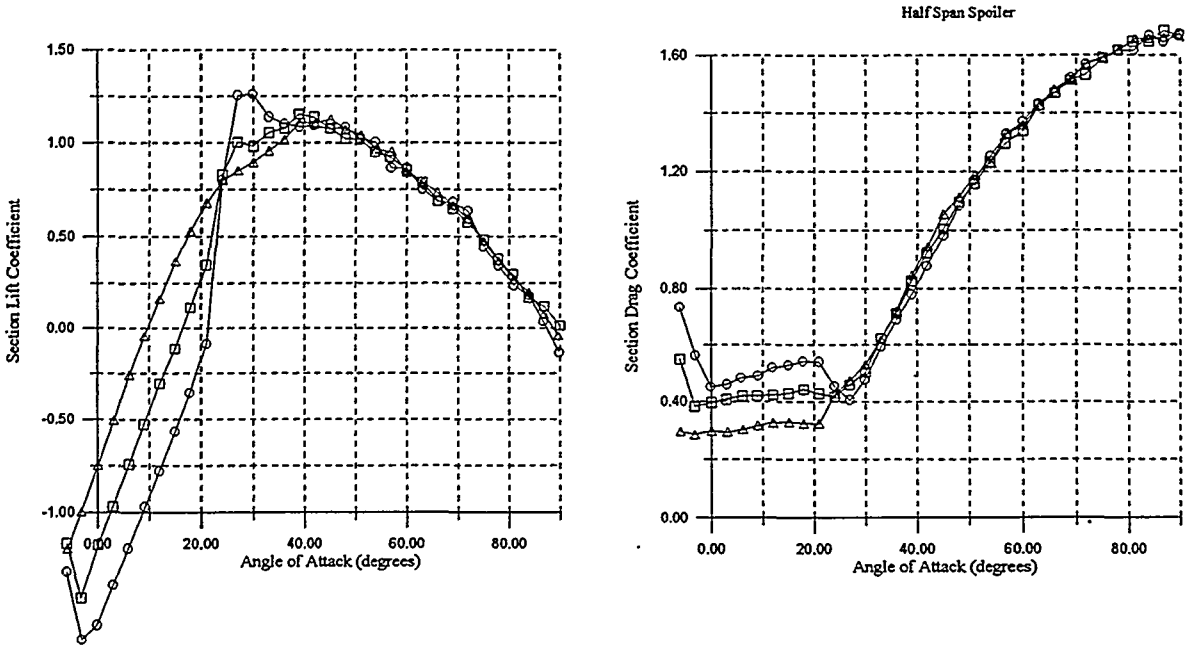

Figures 20b and 20c. Lift and drag coefficient behavior for the Airfoil-Spoiler configuration.

Control Comparisons

To this point in the presentation of results, basic information on the performance of individual controls has been provided. In the following sections, a one-to-one comparison between test configurations is provided.

NACA-Type Control Comparisons

Figure 21 compares the suction coefficient behavior of the NACA Double Split-Flap/60 and Double Split-Flap/112 (Clam-Shell) airfoil control configurations. As can be seen, the Double Split-Flap/60 appears to provide better overall performance as a result of its more negative suction and flatter curve shape. The Double Split-Flap/112 brake is better only for a small angle-of-attack range, between about 20° and 30°.

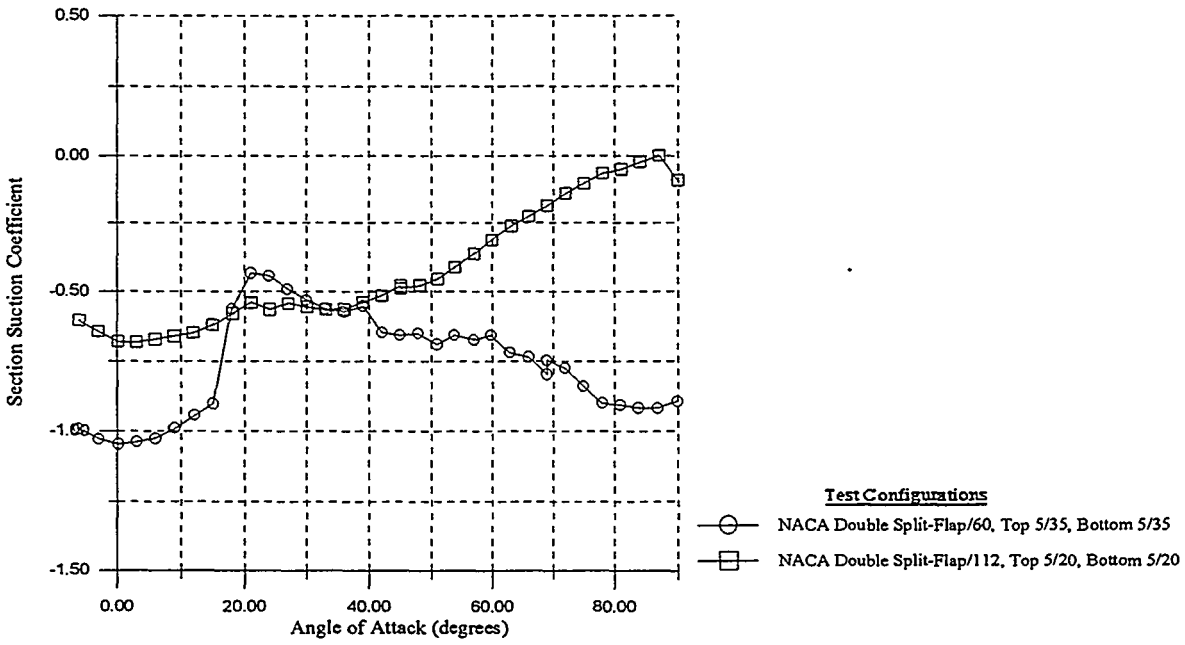

Figure 21. Suction coefficient comparison between NACA Double Split-Flap/60 and Double Split-Flap/112 (Clam-Shell) configurations.*

* *The number-slash pairs indicate percent chord gap and control length used (i.e., 5/35 means a 5% gap and a 35% control length configuration).*

Flap- or Aileron-Type Controls

Figure 22 compares the Spoiler-Flap, "Smooth-Shoulder," and Negative-Camber devices for a 10° control deflection. As can be observed, the aerodynamic control potential of the Smooth-Shoulder airfoil is less than that of the other two configurations. The Spoiler-Flap and the Negative-Camber devices offer very similar performance capabilities; the Spoiler-Flap offers slightly better potential for most of the angle-of-attack range.

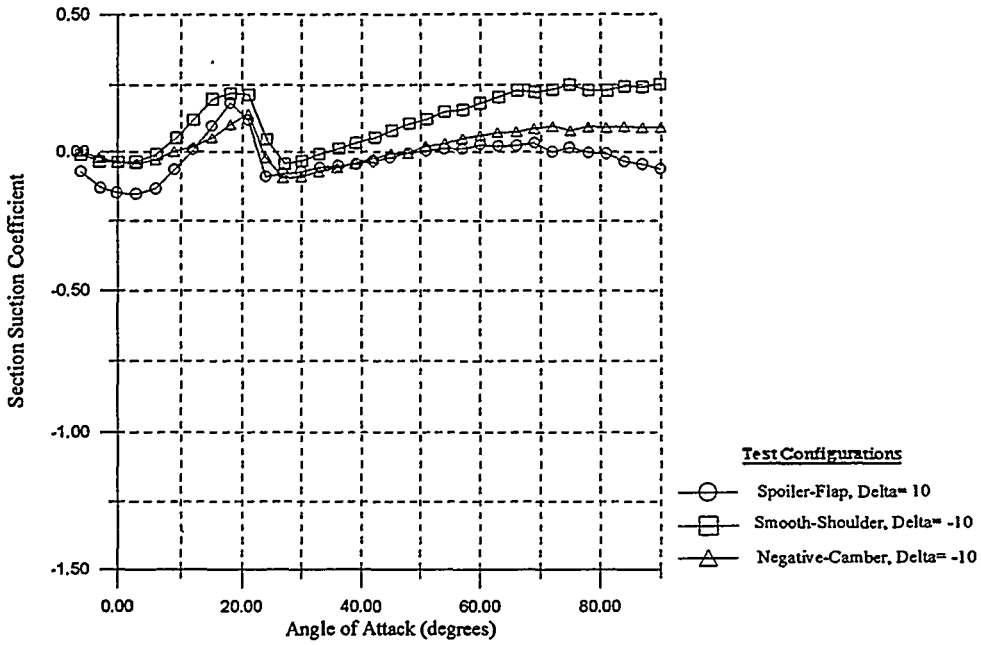

Figure 22. Trailing-edge-type control comparisons for control deflections of 10°.

Figure 23 compares the performance of these particular devices with control deflections of +/-90°. Interestingly, the Smooth-Shoulder control offers superior braking potential at angles of attack between 10° and 30° degrees. However, the Smooth-Shoulder control performs significantly worse for angles of attack greater than 30°, where both the Spoiler-Flap and Negative-Camber controls are superior. The Spoiler-Flap appears to be the better choice between these two control configurations because of predominately more negative suction coefficient behavior.

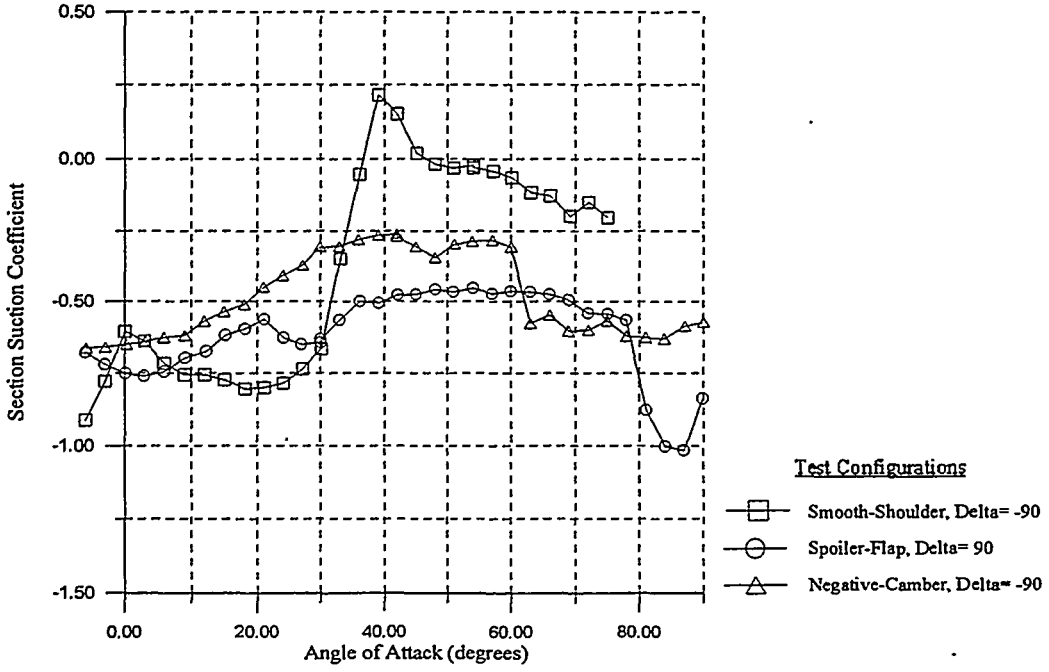

Figure 23. Trailing-edge-type control configuration comparisons for deflections of 90°.

Overall Comparisons

Figure 24 provides a comprehensive suction coefficient comparison for all of the basic configurations examined during this investigation. As is shown, each control produced negative suction coefficients for the entire angle-of-attack range, except for the Smooth-Shoulder between about 35° and 45°. The performances of the NACA Double Split-Flap/60 and the Spoiler-Flap configurations appear to stand out in comparison to the other three controls. The Double Split-Flap/60 is clearly superior for all angles of attack, except between approximately 20° and 35°. The Spoiler-Flap offers a flatter, or more constant, variation of the suction coefficient with angle-of-attack. Interestingly, the Smooth-Shoulder offers the best overall performance between about 15° and 30° angle of attack.

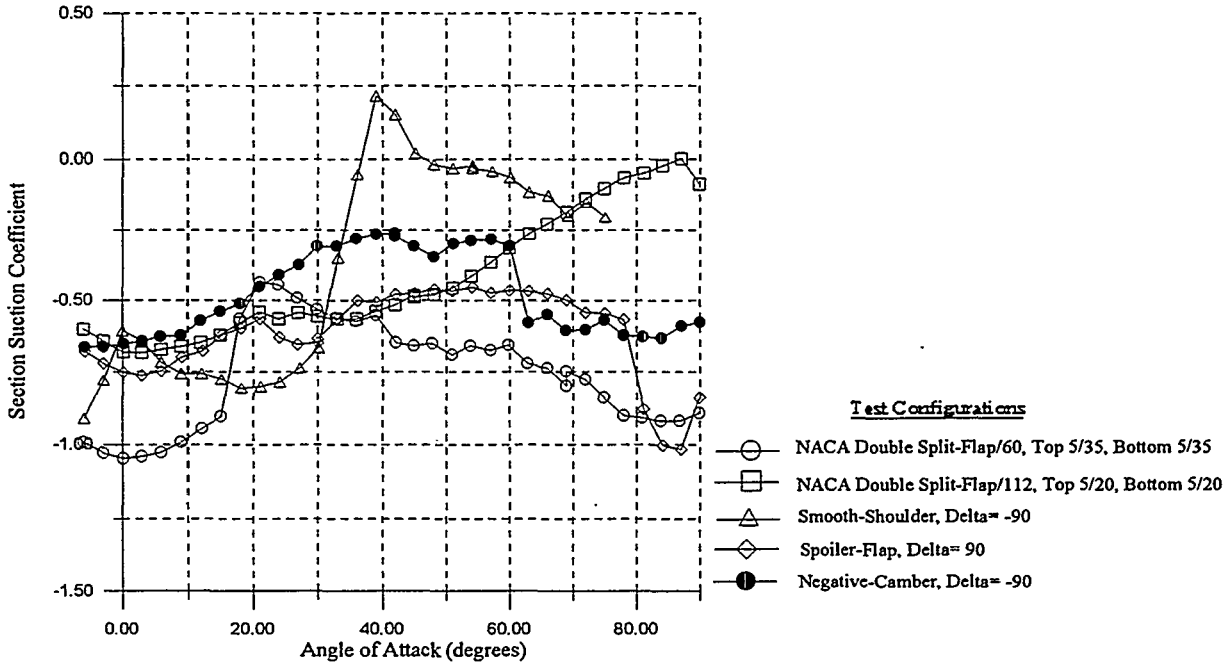

Figure 24. Overall performance comparison for the five configurations examined.*

* *The number-slash pairs indicate percent chord gap and control length used (i.e., 5/35 means a 5% gap and a 35% control length configuration).*

Wake Survey Tare and Interference

Figure 25 shows the results of the wake velocity profile surveys. Specifically, three curves are shown illustrating the wake calculated and wind tunnel balance measured drag behavior of the Negative-Camber control configuration, with control deflection equal to zero. As was discussed previously, the difference between these two curves defines the variation of the model tare and interference drag. Figure 25 shows that the tare and interference drag coefficients are approximately constant and equal to 0.020 for the examined angle of attack range. Data for angles of attack greater than 15° were not obtained as a result of a growing extent of separated flow over the test airfoil. Unfortunately, the wake survey drag calculations become less accurate as the amount of separated flow increases and, as a result, the tare and interference drag coefficient value will be assumed constant for angles of attack greater than 15°.

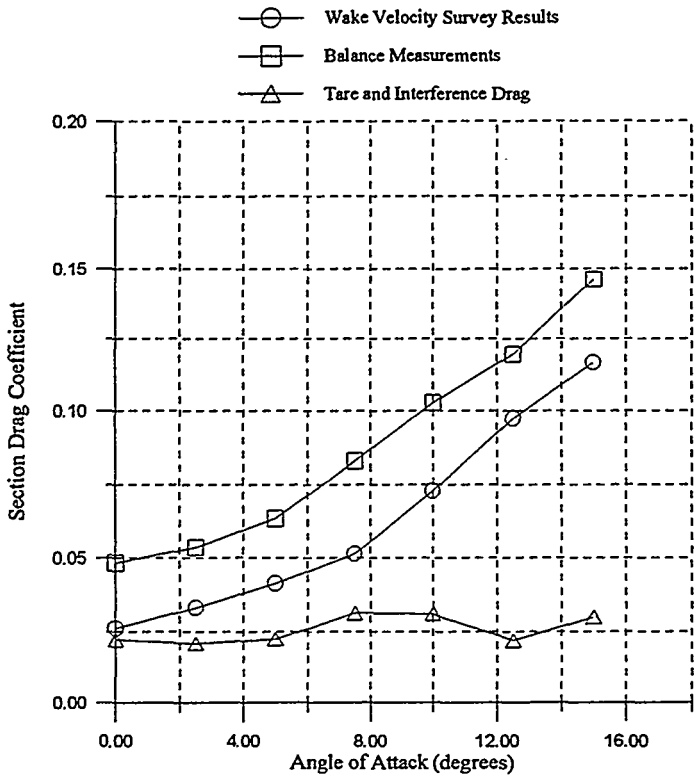

Figure 25. Tare and interference drag as a function of angle of attack.

Figures 26a, 26b, and 26c identify the impact of the tare and interference drag on the suction coefficient data previously presented for the Spoiler-Flap configurations, with 0°, 30°, and 90° control deflections, respectively. As is shown, correcting for the tare and interference drag affected the suction coefficients by a small or essentially insignificant amount. Apparently, the wind tunnel model installation had less tare and interference drag than anticipated.

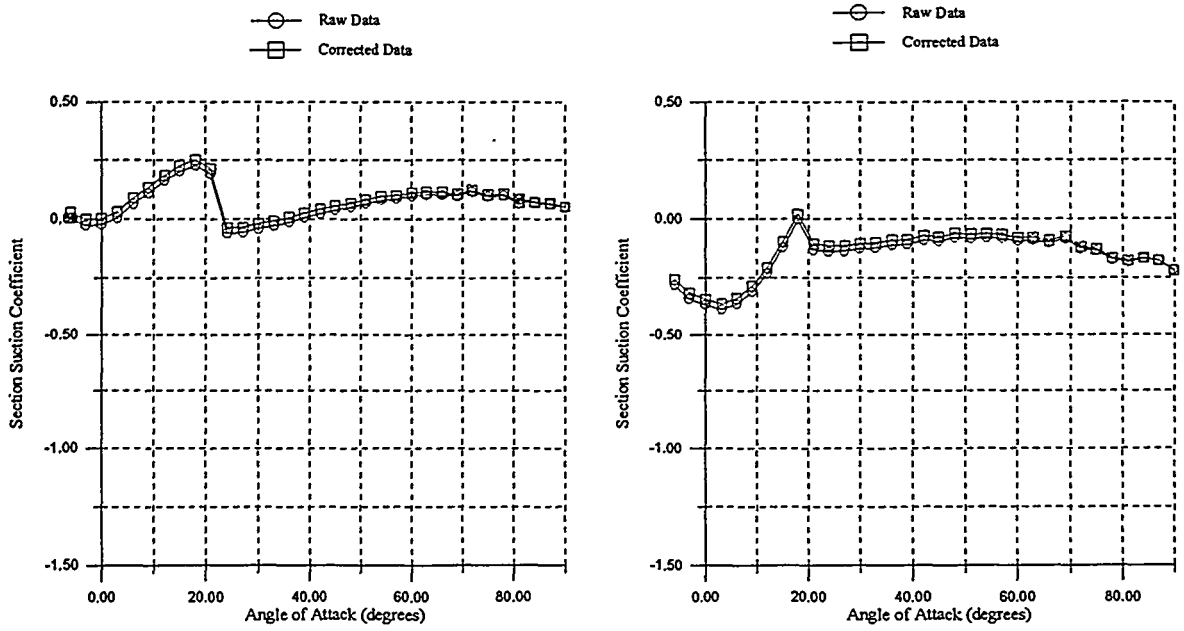

Figures 26a and 26b. Spoiler-Flap suction coefficient tare and interference effect for Delta 0.0° and 30°.

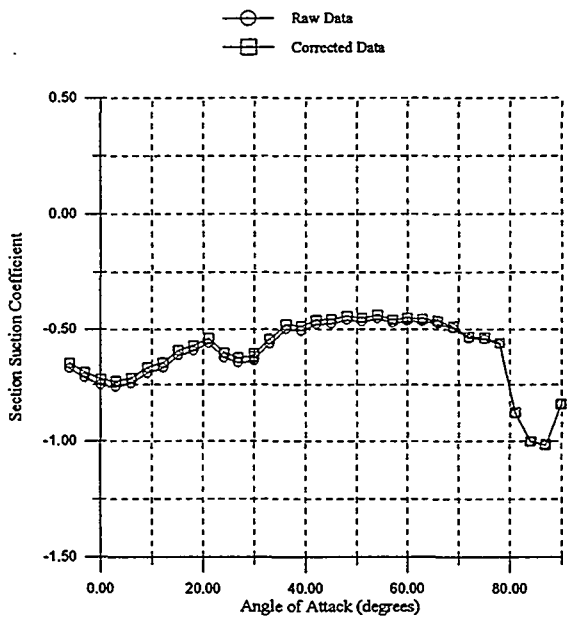

Figure 26c. Spoiler-Flap suction coefficient tare and interference effect for Delta 90.0°.

Static Pressure Distributions

Static pressure distributions about the Spoiler-Flap and Negative-Camber configurations were obtained for three control deflections over a wide angle-of-attack range. The following figures present selected results, because inclusion of all of the data would consume a large amount of space. Only six angle-of-attack conditions are shown on each plot.

Static pressure distributions for the Spoiler-Flap and Negative-Camber configurations are shown in Figures 27a, 27b, and 27c and in Figures 28a, 28b, and 28c, respectively. A solid line indicates pressures for the upper surface of the airfoil or control element, while a dashed line indicates pressures for the lower surfaces. Data to the left and right of the 50% chord location identify the main and control element portions of the airfoil, respectively.

A detailed discussion of each set of static pressure data will not be included in this paper. The real value of these plots is for identifying regions of separated flow and for calculation of control hinge moments. Typically, a nearly constant level of static pressure over a portion of the airfoil surface indicates separated flow. As can be seen, each of the control configurations produces significant amounts of flow separation for large control deflections or angles of attack, or both.

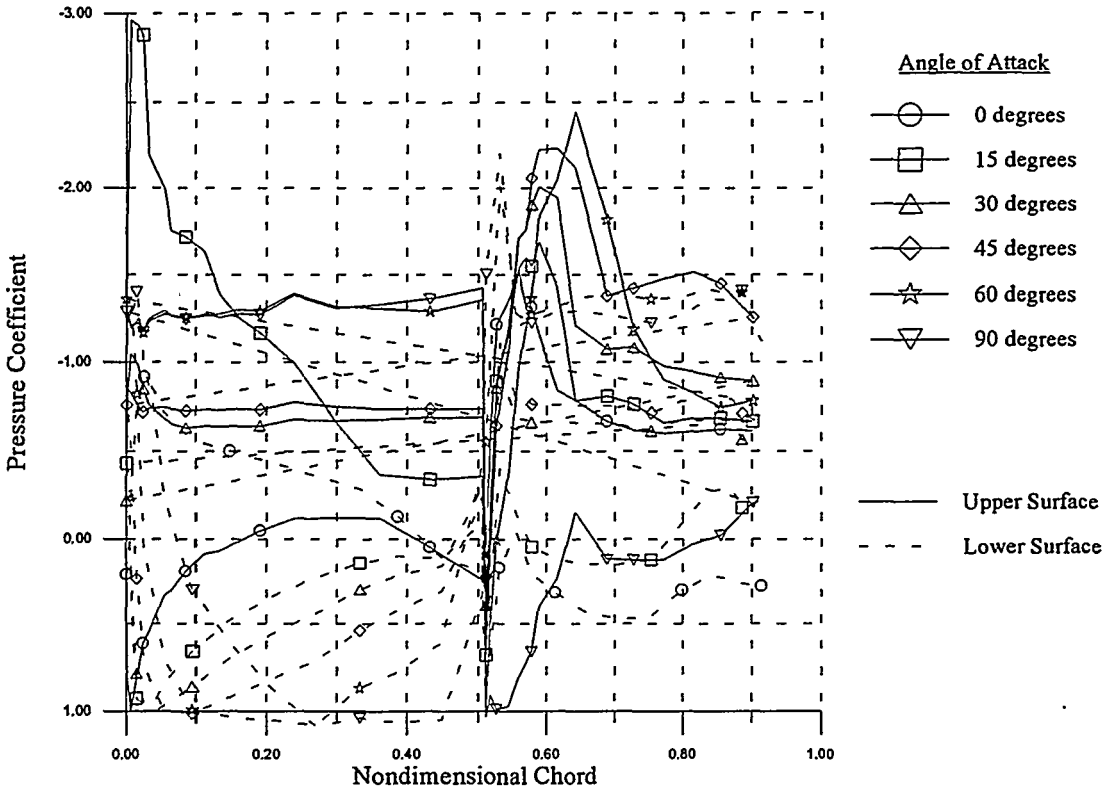

Figure 27a. Static pressure coefficient distribution for the Spoiler-Flap configuration with Delta of 45°.

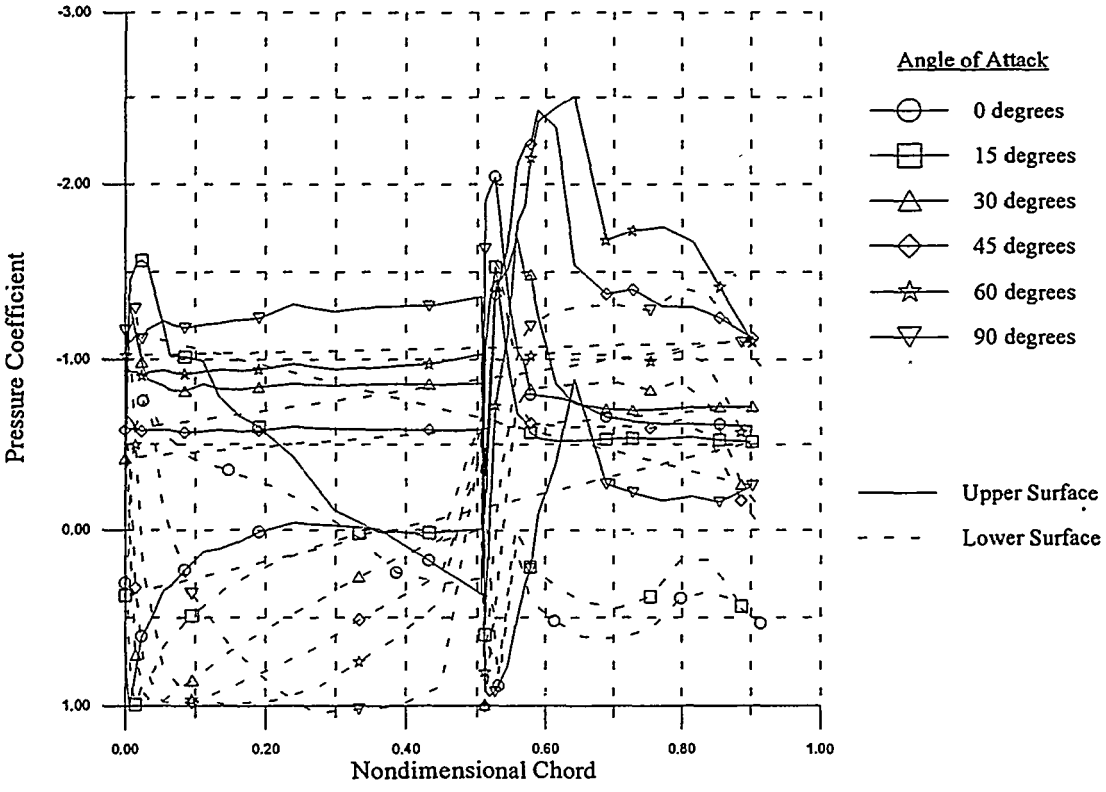

Figure 27b. Static pressure coefficient distribution for the Spoiler-Flap configuration with Delta of 60°.

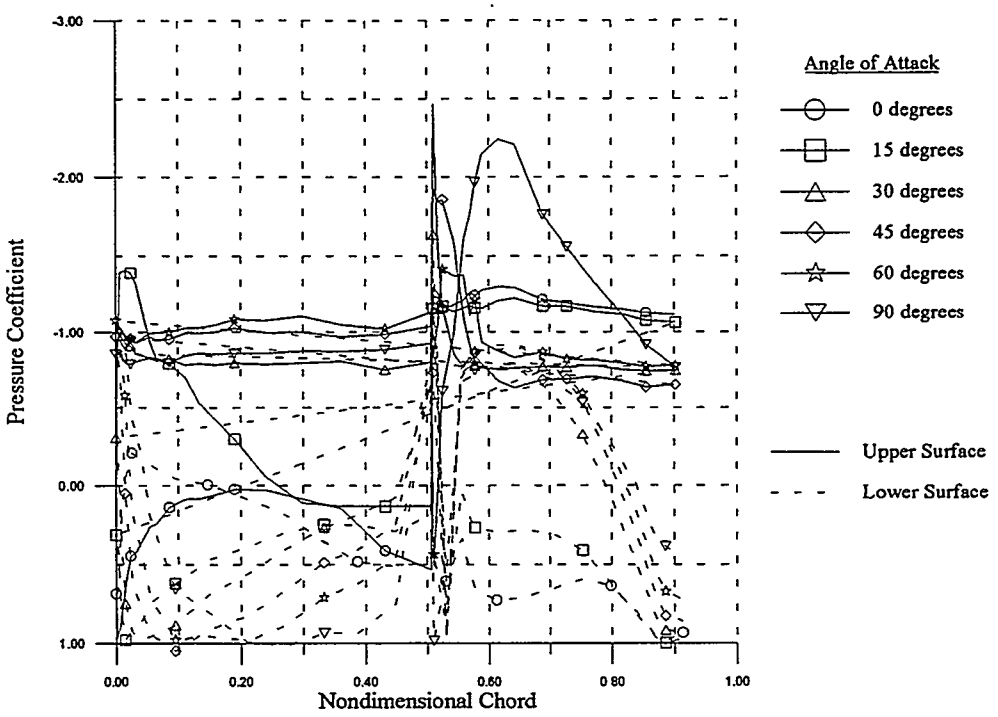

Figure 27c. Static pressure coefficient distribution for the Spoiler-Flap configuration with Delta of 90°.

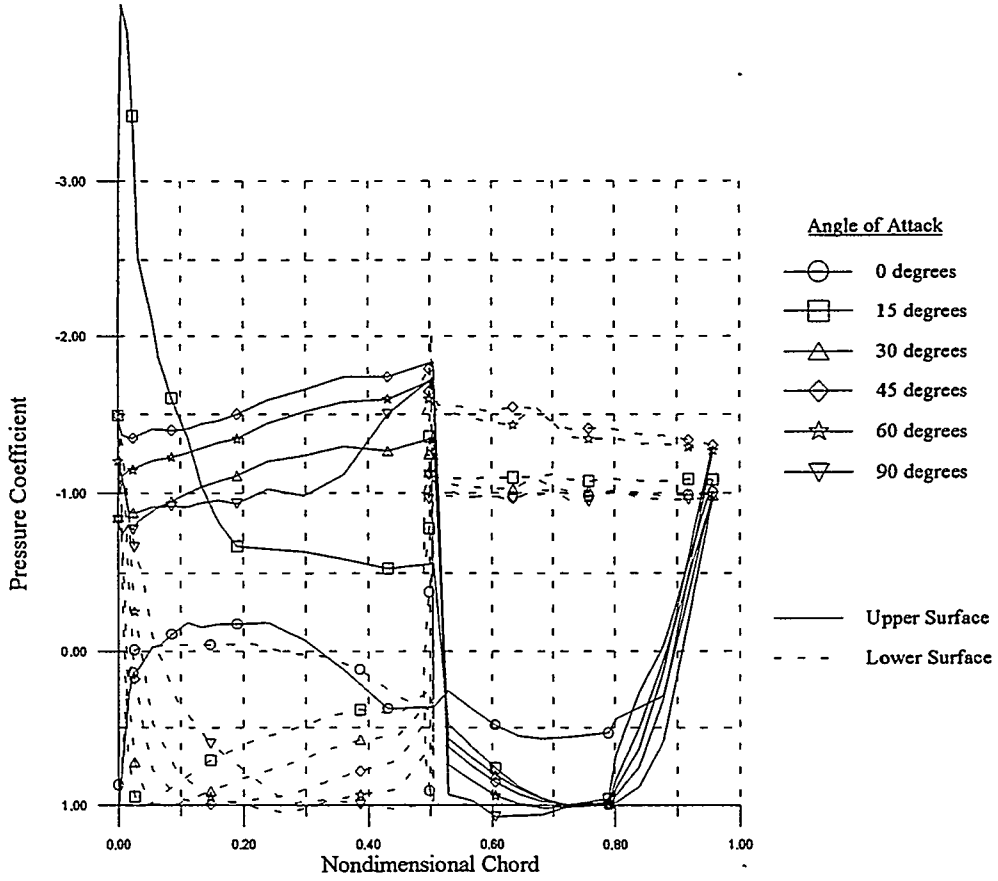

Figure 28a. Static pressure coefficient distribution for the Negative-Camber configuration with Delta of -45°.

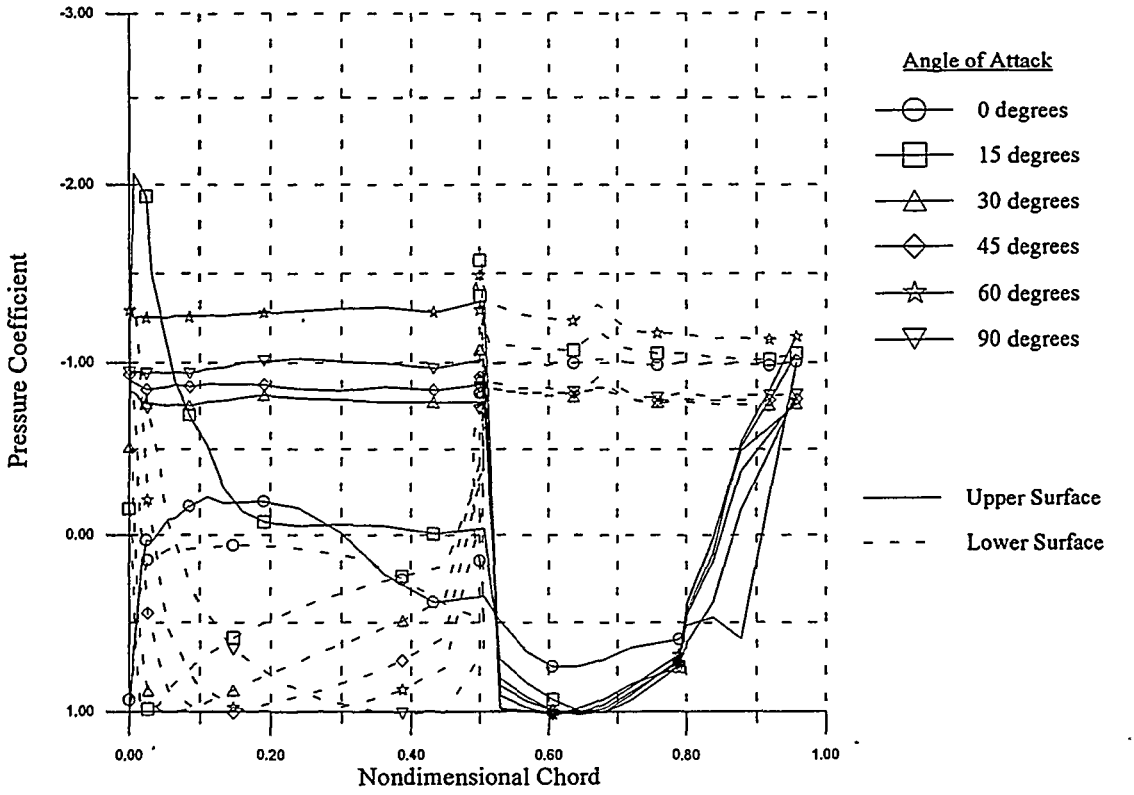

Figure 28b. Static pressure coefficient distribution for the Negative-Camber configuration with Delta of -60°.

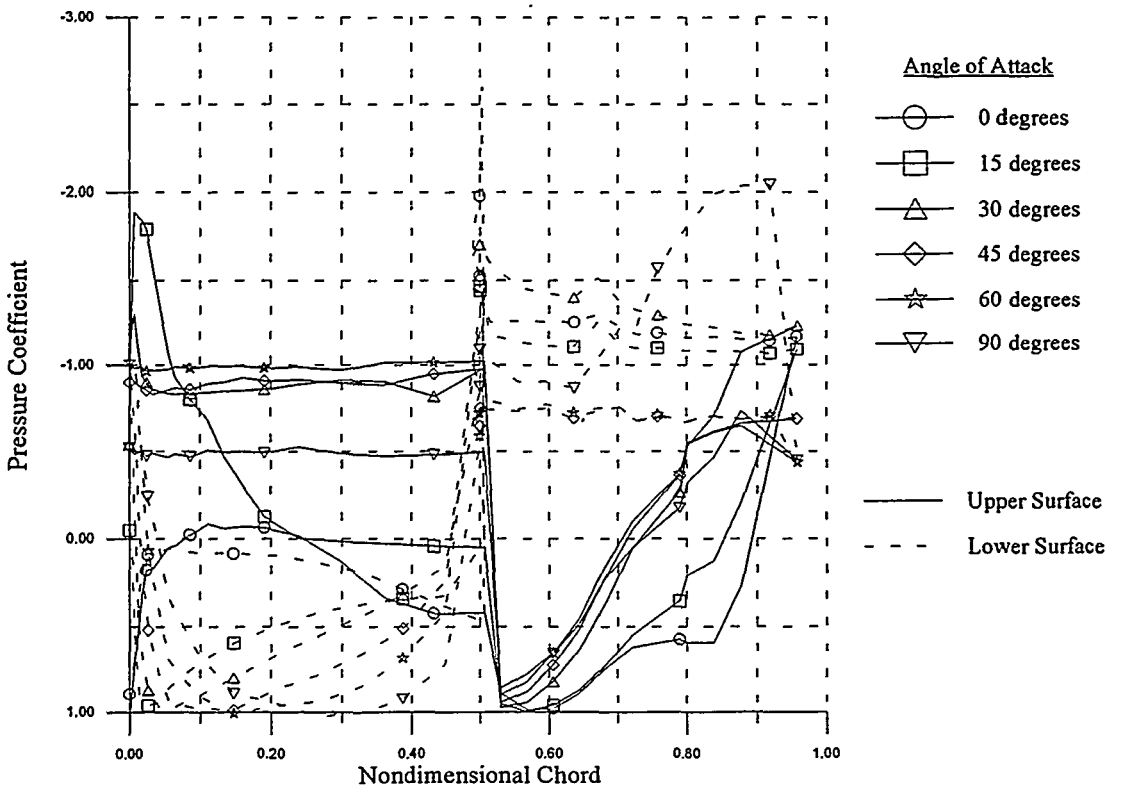

Figure 28c. Static pressure coefficient distribution for the Negative-Camber configuration with Delta of -90°.

Hinge Moments

The control surface static pressure distributions were integrated, using the methods outlined in Rae and Pope (1984), to identify hinge or actuation moment coefficients. The results of these efforts are shown in Figures 29 and 30. As was discussed earlier, a total of 30 static-pressure taps were fit to the test model at approximately equal intervals around the control surface. In retrospect, it would have been advisable to have included more than 60 pressure taps, as this would have improved the accuracy of the hinge-moment calculations. Unfortunately, an exact measure of this potential effect is impossible to identify.

Figures 29 and 30 show that the moment coefficients vary notably as a function of angle of attack and control deflection. The control hinge-moment coefficient (Cm_h) is given as follows:

$$Cm_h = (M_c)/(q)(c_c^2)$$

where M_c is the control hinge moment defined via the integration, q is the local dynamic pressure, and c_c is the control chord length. A positive moment coefficient indicates a clockwise (i.e., trailing-edge down) torque is applied to the control.

As Figure 29 shows, it appears that the Spoiler-Flap control will tend to open automatically for deflection angles less than approximately +45° over the entire angle-of-attack range. As the control deflection increases, negative (i.e., closing) hinge moments develop.

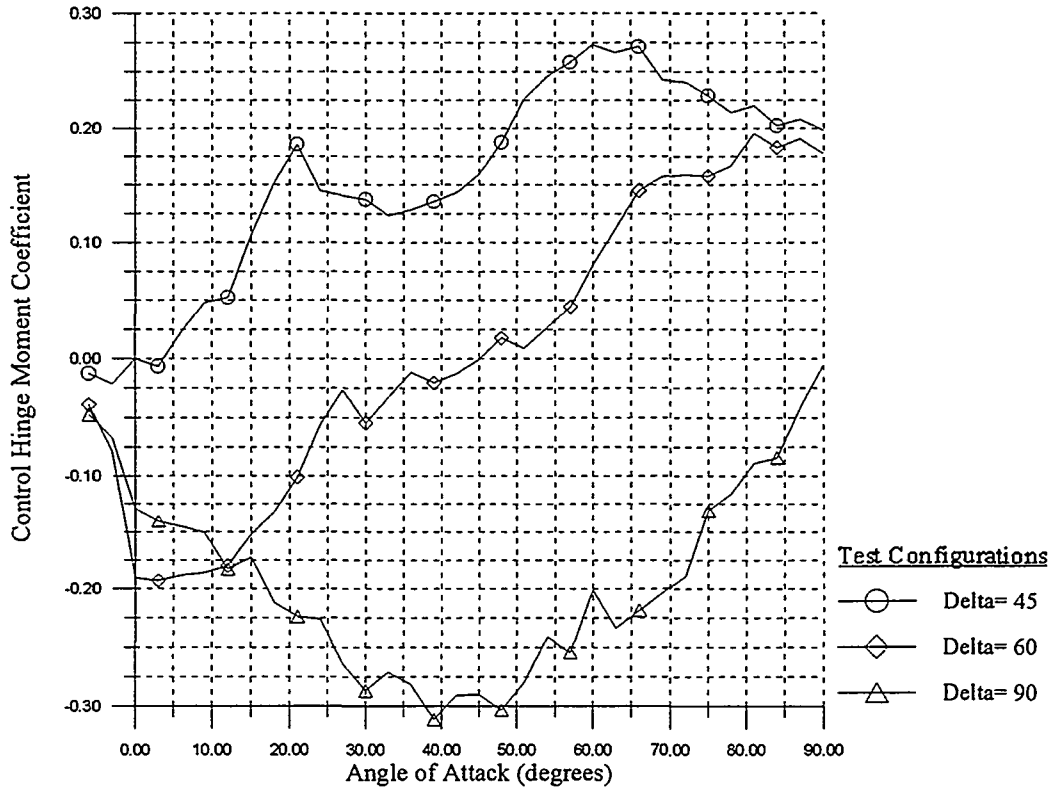

Figure 29. Spoiler-Flap control hinge-moment coefficient as a function of deflection angle. (Moment is about the control pivot point and clockwise-positive.)

Figure 30 indicates that the Negative-Camber hinge moment coefficient remains nearly constant and positive for angles of attack greater than approximately 20°, regardless of the control deflection angle. Interestingly, however, the integrated pressure data indicates that the magnitude of the control hinge moment reduces as the control deflection increases.

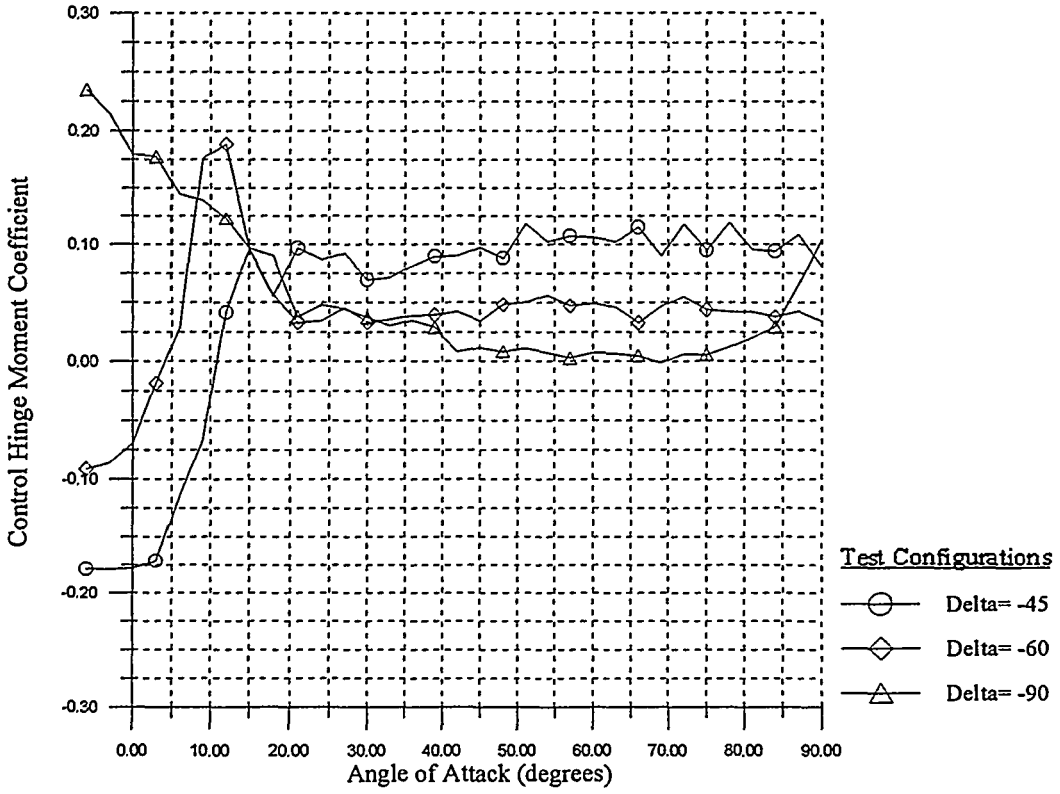

Figure 30. Negative-Camber control hinge moment variation as a function of deflection angle. (Moment is about the control pivot point and clockwise-positive.)

WIND Code Performance Evaluations

A computerized turbine performance analysis was conducted to further evaluate the potential rotor overspeed control capability of the various trailing-edge devices. Actual wind turbine geometry and operating parameters were specified to represent some common 300-kW-class wind turbines currently offered by various manufacturers. The braking potential of each control was then evaluated numerically for a wide range of operating conditions.

Turbine Geometry

The evaluation turbine was specified as having a two-bladed rotor with a radius of 41 feet and a hub cut-out radius of 2 feet. The blade chord and twist distributions, shown in Figures 31a and 31b respectively, were set to optimize performance at an operating speed of 60 rpm, and to allow a cut-in wind velocity of about 11 miles per hour. Each aerodynamic control occupied 30% of the rotor span and was positioned between the 65% and 95% span locations. As was examined during the wind tunnel tests, all controls were of 50% chord.

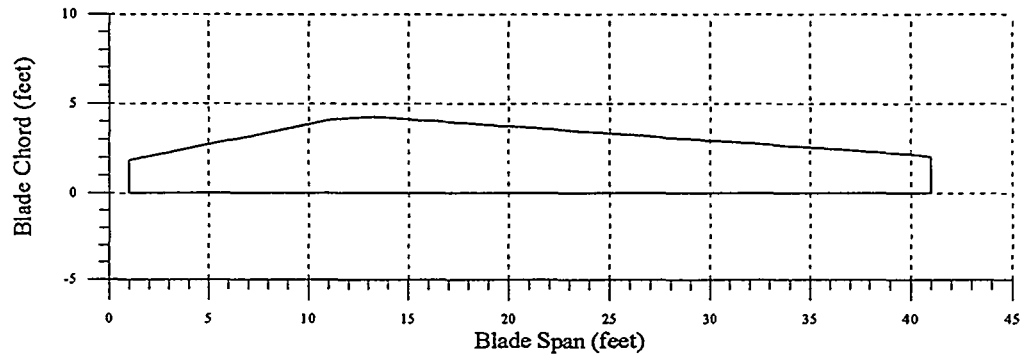

Figure 31a. Blade chord distribution for the evaluation turbine.

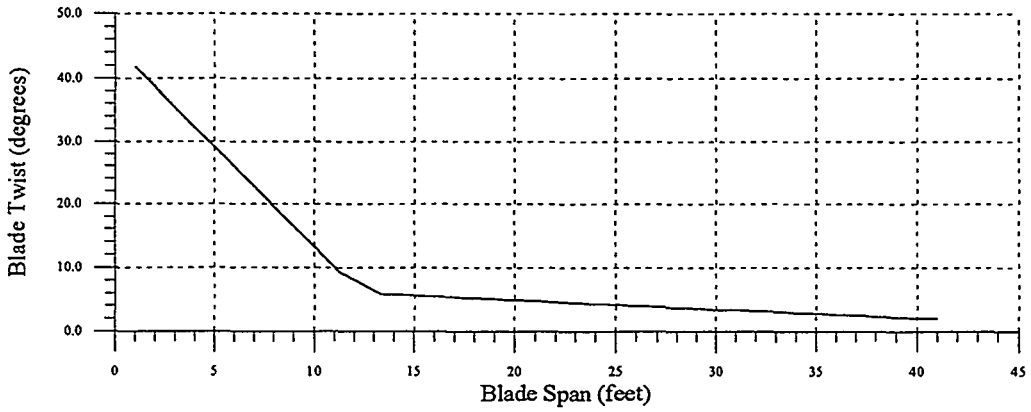

Figure 31b. Blade twist distribution for the evaluation turbine.

Turbine Performance Analysis

Along with the turbine geometry information, aerodynamic control data (corrected for tare and interference drag) obtained during the wind tunnel tests were input into a new version of the *WIND II* code (Snyder and Staples 1982). This particular program, developed at WSU, performs a detailed wind turbine performance analysis given relevant geometric and aerodynamic data. Most importantly, the code includes features that make it well suited to the analysis of turbines with controls, using a personal computer and a simplified input scheme. (A publication detailing this new code, to be called *WIND III*, will be released shortly.)

A number of different types of output are available from the *WIND* code, but for the current investigation the variation of rotor torque (C_q) as a function of tip-speed ratio (X) was of most interest. These results provide direct insight into the ability of a given control configuration to affect the wind turbine rotation speed and power output.

Individual Results Summary

Figure 32 shows the torque coefficient performance of the NACA Double Split-Flap/60 control for various symmetrical brake gap and length combinations. As can be observed, the zero gap and 40% length control is capable of producing the largest braking torque coefficients. This result is consistent with the suction coefficient data identified previously from the two-dimensional airfoil tests. For all examined tip-speed ratios and control subconfigurations, the torque coefficient was negative.

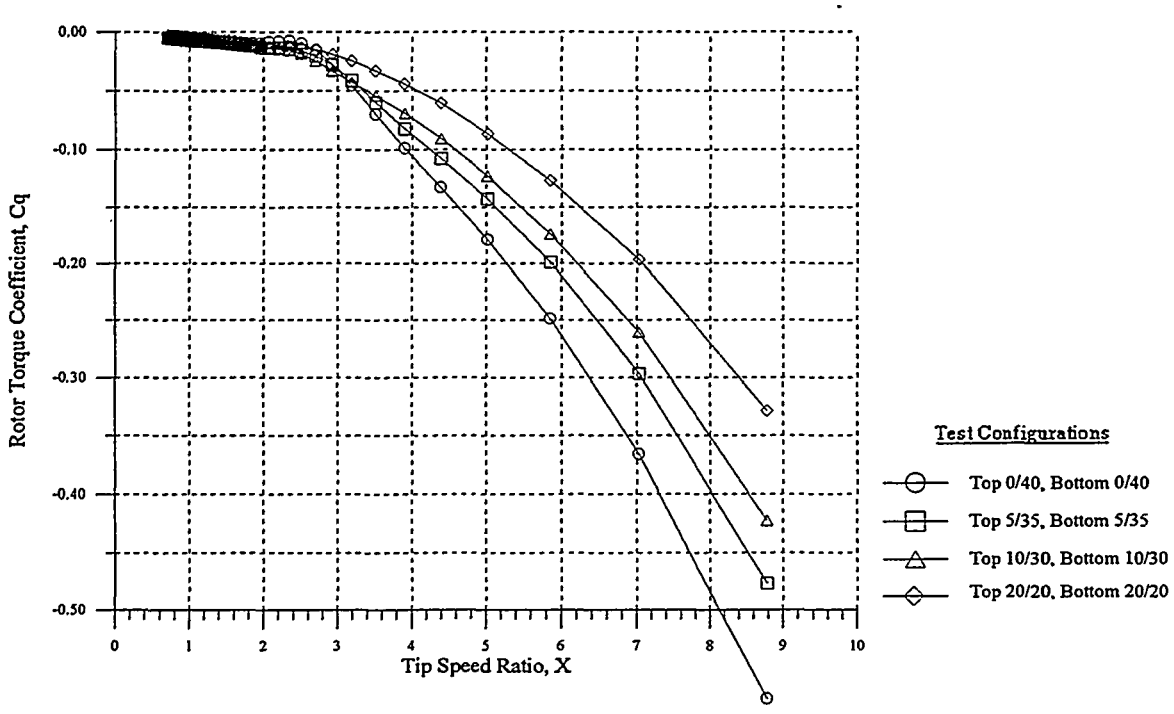

Figure 32. Effect of NACA Double Split-Flap/60 configurations on turbine torque.*

** The number-slash pairs indicate percent chord gap and control length used (i.e., 5/35 means a 5% gap and a 35% control length configuration).*

The torque performance of the NACA Double Split-Flap/112 (Clam-Shell) configuration is identified in Figure 33. These results indicate that a 5% gap and 20% length brake panel offer the best braking capabilities. Again, this plot agrees with the results observed previously. For all examined tip-speed ratios and control subconfigurations, the torque coefficient was negative.

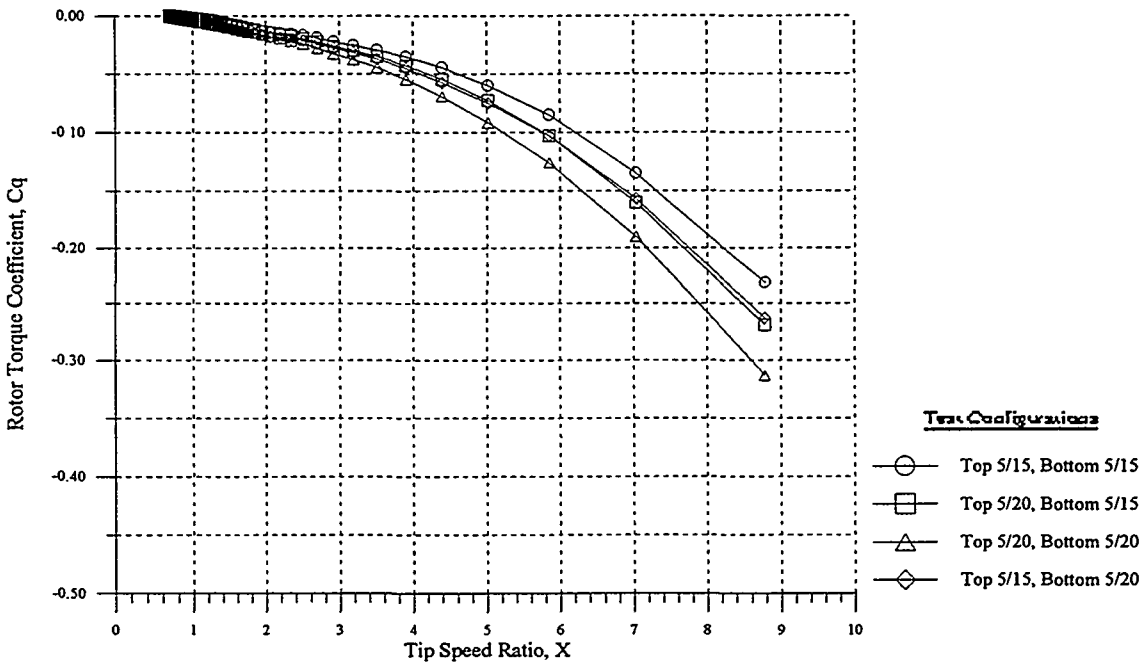

Figure 33. Effect of NACA Double Split-Flap/112 (Clam-Shell) brake configurations on turbine torque.*

* *The number-slash pairs indicate percent chord gap and control length used (i.e., 5/35 means a 5% gap and a 35% control length configuration).*

Figures 34, 35, and 36 illustrate the braking potential for the Smooth-Shoulder, Spoiler-Flap, and the Negative-Camber control configurations, respectively, as a function of control deflection angle. In each case, it appears desirable to deflect the control fully to the 90° condition in order to produce the maximum negative rotor torque coefficients. Detailed study of the *WIND* code results indicates, for the values examined, that a deflection of +/-60° is necessary for each of these controls to produce a torque coefficient that is less than or equal to zero over the entire tip-speed ratio range.

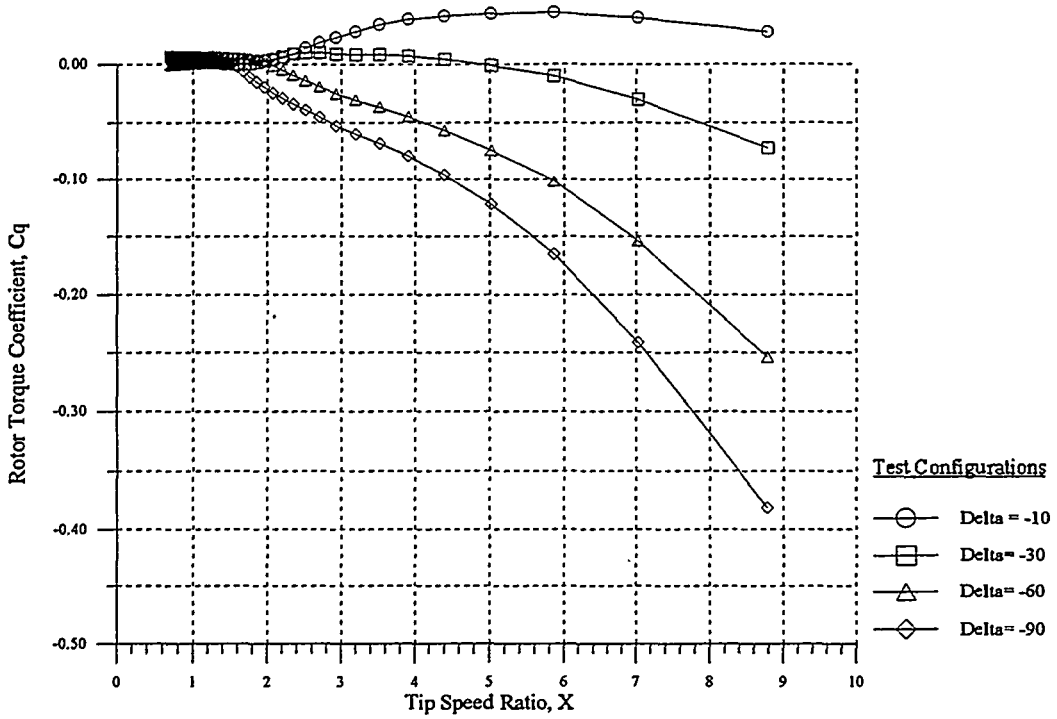

Figure 34. Impact of Smooth-Shoulder control deflections on turbine torque.

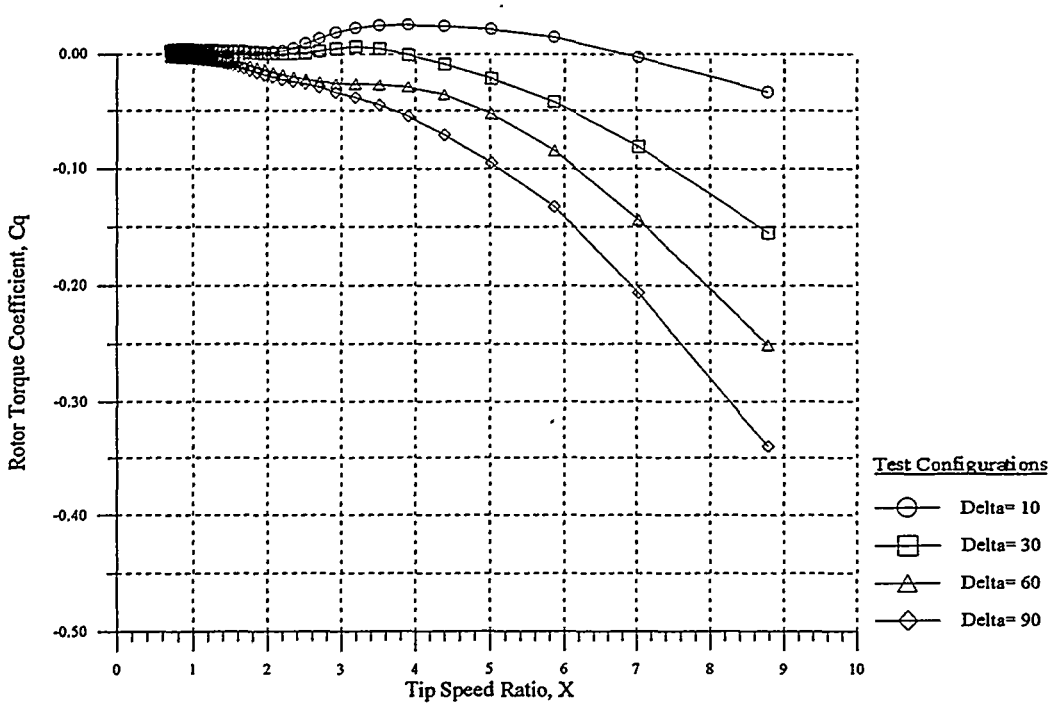

Figure 35. Impact of Spoiler-Flap control deflections on turbine torque.

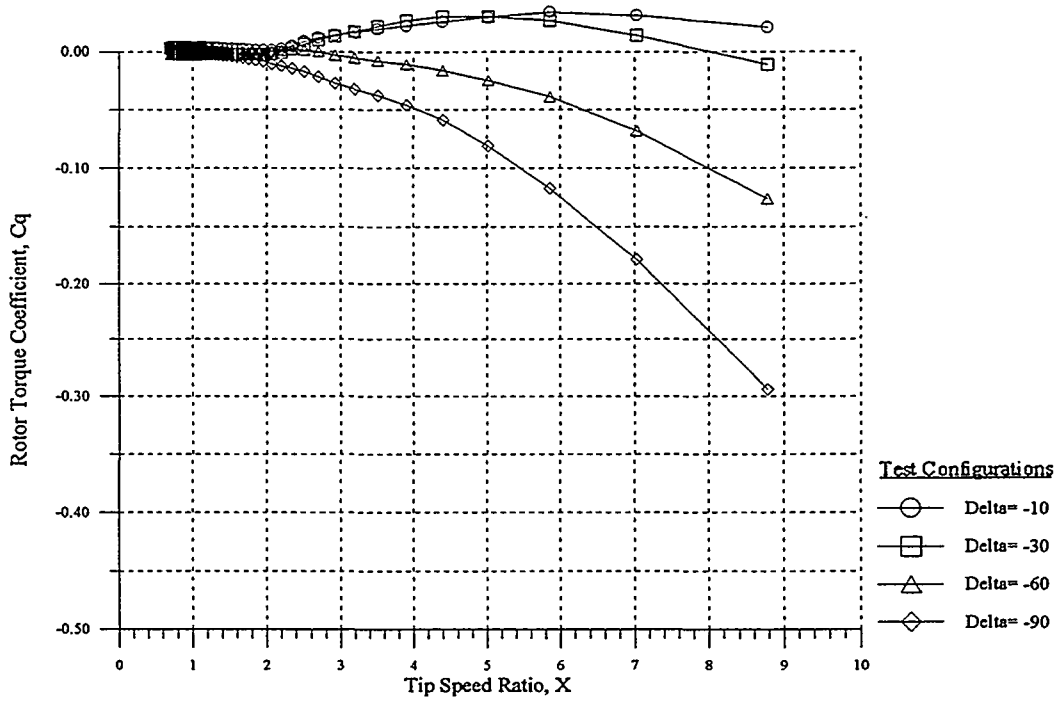

Figure 36. Impact of Negative-Camber control deflections on turbine torque.

Figure 37 compares the relative performance of each of the best control configurations studied. Interestingly, despite the more constant variation of the Spoiler-Flap suction coefficient over a wide angle-of-attack range, the NACA Double Split-Flap/60 configuration appears to offer better overall braking performance at tip-speed ratios above 3.5 (or for wind speeds less than 50 mph).

Closer examination of these results, at the lowest tip-speed ratio conditions, provides further insight into the capabilities of each of these controls for rotor braking in high-wind situations. Specifically, as Figures 38a and 38b show, the NACA Double Split-Flap/60 performs poorly at tip-speed ratios between about 2.0 and 3.0 (or between wind speeds of about 59 and 88 mph). In contrast, the Smooth-Shoulder configuration performs notably better than the other four configurations at tip-speed ratios between about 1.8 and 3.4 (or winds of 98 and 52 mph). However, below a tip-speed ratio of 1.8 (or wind speeds greater 98 mph), the performance of the Smooth-Shoulder control is worse than all of the other configurations, and the NACA style and Spoiler-Flap configurations appear superior.

An approximate indication of the test rotor angle of attack (at the control midspan location) versus tip-speed ratio is shown in Figure 39. This figure shows that the rotor controls operate at increasing angles of attack as the tip-speed ratio drops (or as the wind speed rises). This information and the aerodynamic data shown in Figure 24 confirm that the trailing-edge control with the most negative suction coefficient, at a given operating angle-of-attack condition, produces the greatest braking torque.

Based on the results shown in Figures 37 and 38, all of the controls should offer reasonable power modulation capabilities. However, the NACA Double Split-Flap/60, Double Split-Flap/112, and the Spoiler-Flap configurations appear to offer the most consistent braking capabilities over the widest and the most important (low) tip-speed ratio range.

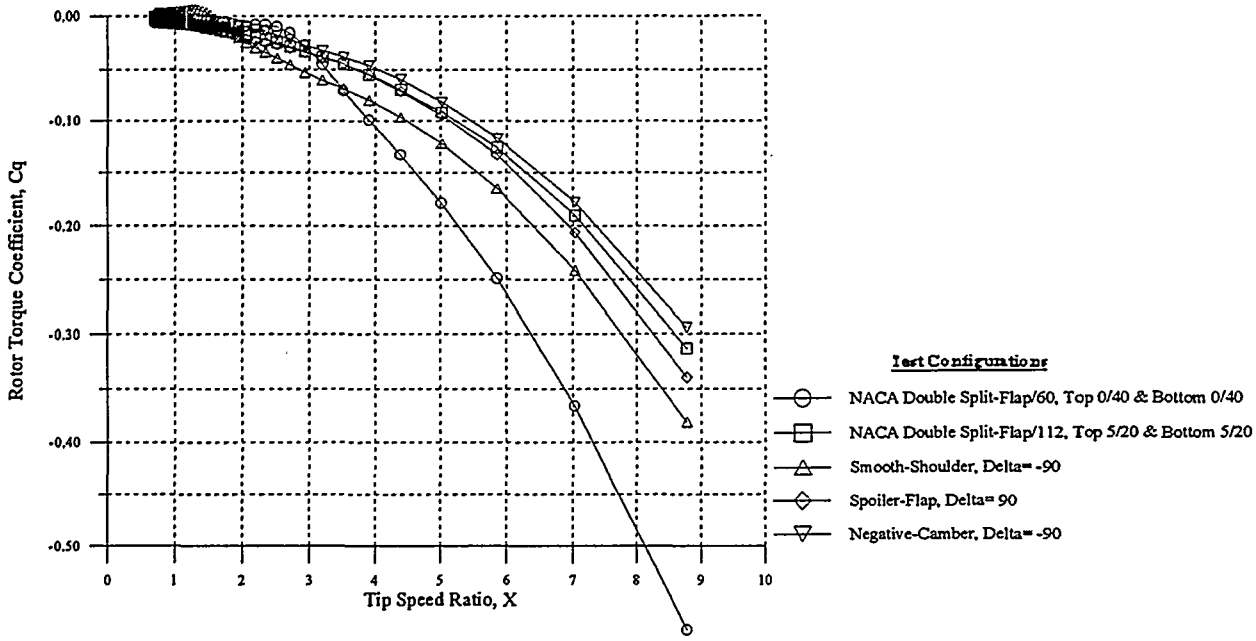

Figure 37. Overall performance comparison for the five controls evaluated.*

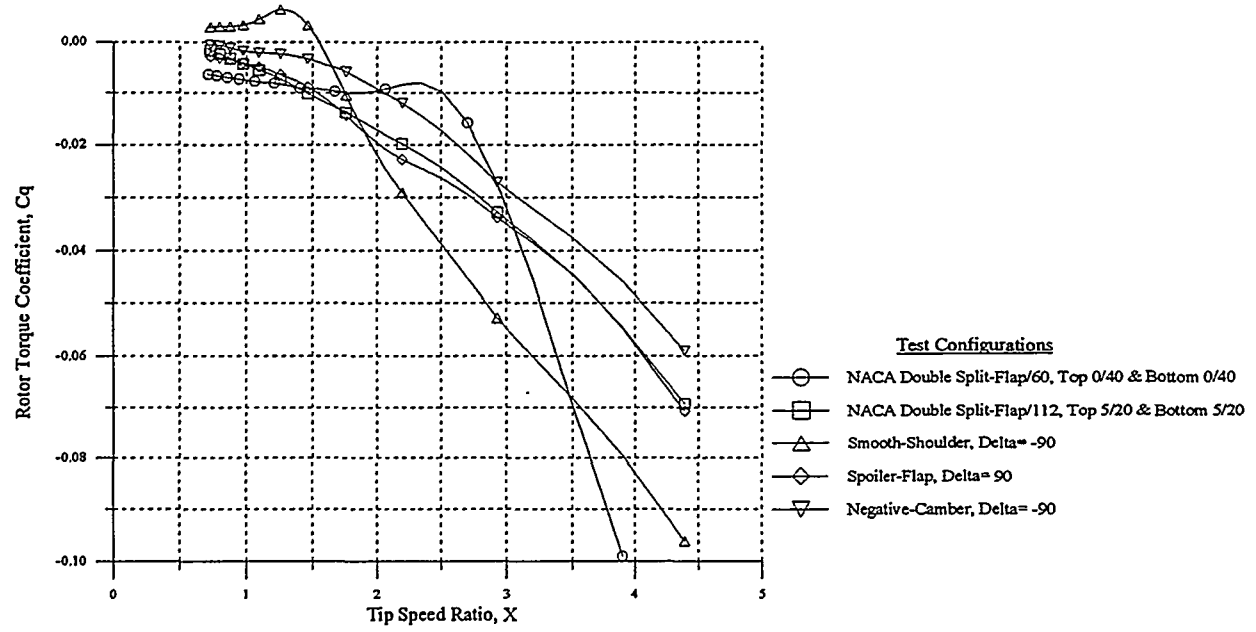

Figure 38a. Torque behavior of each control over a low-tip-speed ratio range.*

* *The number-slash pairs indicate percent chord gap and control length used (i.e., 5/35 means a 5% gap and a 35% control length configuration).*

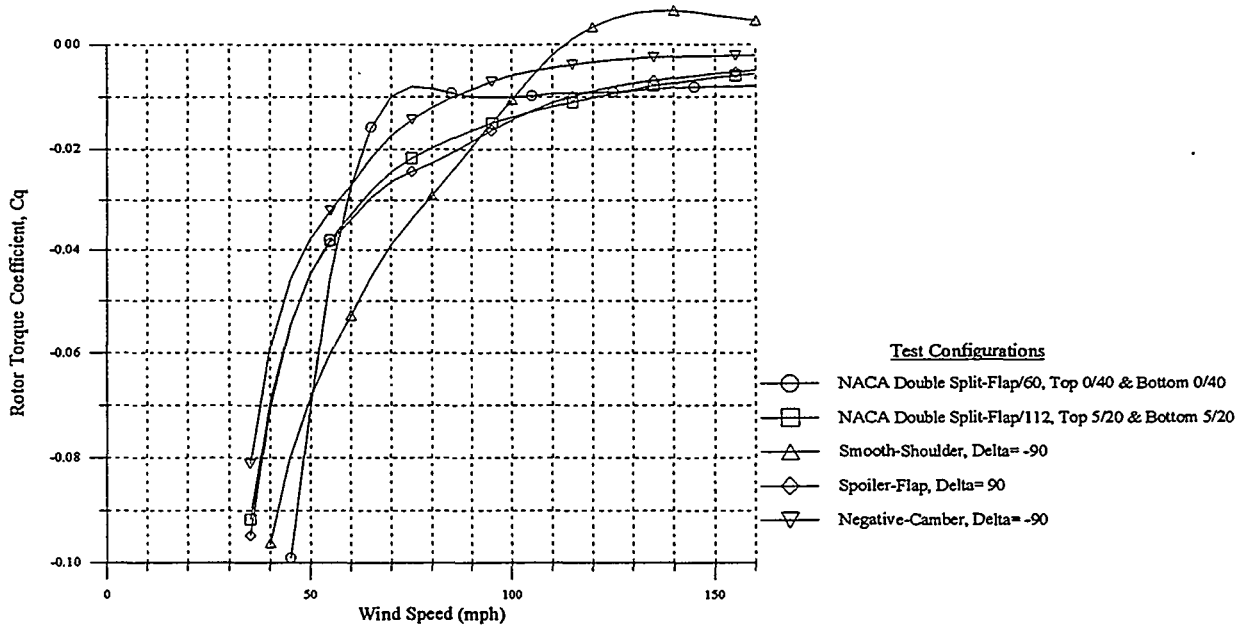

Figure 38b. Torque behavior of each control as a function of wind speed.*

* *The number-slash pairs indicate percent chord gap and control length used (i.e., 5/35 means a 5% gap and a 35% control length configuration).*

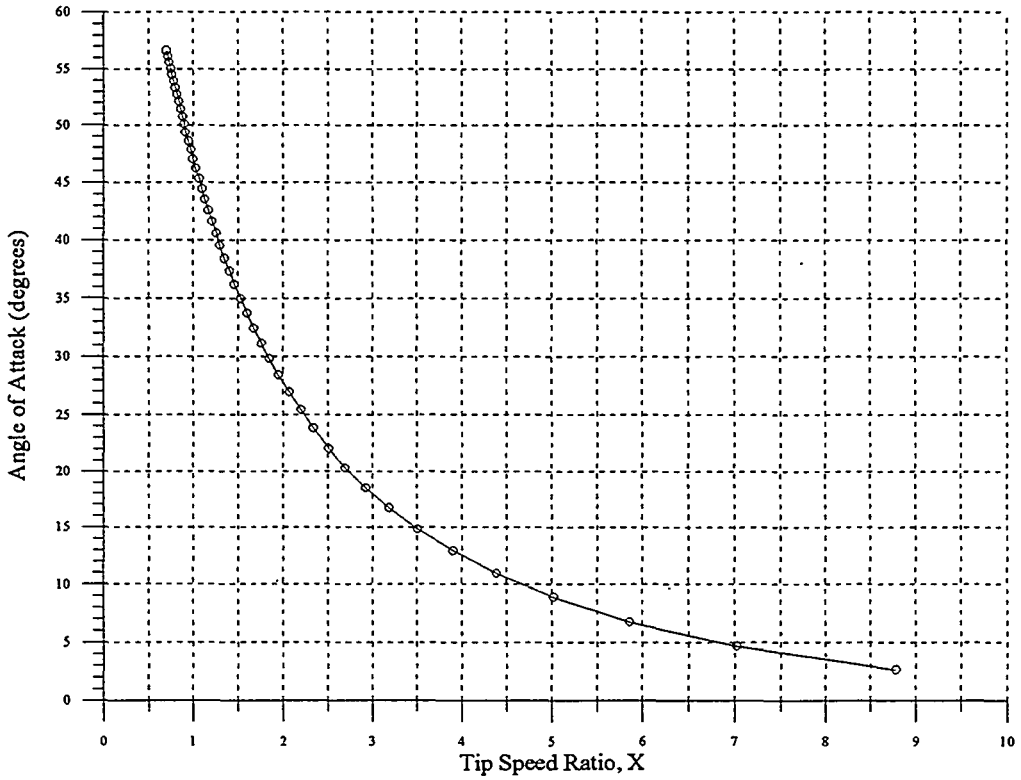

Figure 39. Approximate operating angle of attack, at the 82.5% blade span location, as a function of tip-speed ratio.

Conclusions and Recommendations

An investigation was undertaken to identify the aerodynamic performance of five separate airfoil trailing-edge control devices and to evaluate their potential for wind turbine power modulation and overspeed protection. A modular two-dimensional wind tunnel model was constructed and examined during extensive wind tunnel testing. Aerodynamic force, moment, and pressure data were acquired and analyzed for various control configurations, subconfigurations, and angles of attack. Suction coefficient data indicated the relative performance of each trailing-edge control. To better interpret their potential performance, the controls were evaluated numerically using a generic wind turbine geometry and a turbine performance analysis computer program. Based on the results of this investigation, the following conclusions and recommendations are offered.

1) The NACA Double Split-Flap/60 and Spoiler-Flap configurations produce the largest negative suction coefficients over the broadest angle-of-attack range.

2) Performance analysis, based on two-dimensional data, indicates that all of the examined 30% span controls will produce negative rotor torque at tip-speed ratios greater than about 2.0 (i.e., for wind speeds less than 88 mph). At tip-speed ratios below 2.0 (i.e., for winds greater than 88 mph), the NACA Double Split-Flap/60, Double Split-Flap/112, and Spoiler-Flap controls outperform all of the other configurations. As a result, these controls appear best suited for wind turbine overspeed protection applications, given that outstanding low tip-speed ratio capabilities will be of paramount importance.

3) Considering potential structural and mechanical aspects, use of the Spoiler-Flap control configuration on a turbine appears to be an attractive alternative to currently used overspeed-control devices. The NACA Double Split-Flap/112 would likely require a complex actuation mechanism and an elaborate structural means to absorb control opening loads.

4) Blade chord and twist will affect the selection of an appropriate control for turbine overspeed control. Information on the expected angle-of-attack conditions at the location of the proposed control and detailed suction coefficient information will aid in the correct selection of a trailing-edge control device.

5) The current tests were performed at less than full-scale Reynolds number conditions. As a result, there is a need to identify the impact of Reynolds numbers and to obtain corresponding aerodynamic data for turbine design purposes.

6) Further study of three-dimensional flow effects is needed. It is conceivable that the application of the current two-dimensional data might be optimistic with respect to aerodynamic braking.

Recently completed follow-on wind tunnel tests of the Spoiler-Flap configuration investigated the influence of chord, hinge location, and leading-edge shape on device effectiveness. (This work will be documented in an upcoming report.) Future research will focus on validating the Spoiler-Flap aerodynamics by comparing wind tunnel data to data obtained in rotating-frame atmospheric tests conducted at NREL's National Wind Technology Center. Aerodynamic, structural, and mechanical tests on full-scale blades will also be conducted, either in cooperative projects with industry or in connection with NREL advanced component development projects.

References

Johnson, B.L. (1993). *Facility Description of the Walter H. Beech 7X10 Foot Low-Speed Wind Tunnel.* Wichita, KS: Aerodynamic Laboratory, Wichita State University.

Quandt, G.A. (1994). *Wind Turbine Trailing-Edge Aerodynamic Brake Design.* Subcontract Report No. TAD-3-13400. Golden, CO: National Renewable Energy Laboratory.

Rae, W.H.; Pope, A. (1984). *Low-Speed Wind Tunnel Testing* 2nd Edition, New York, John Wiley & Sons.

Snyder, M.H.; Staples, D.L. (1982). *WIND-II Users Manual.* Wind Energy Report No. 15. Wichita, KS: Wind Energy Laboratory, Wichita State University.

Snyder, M.H.; Wentz, Jr., W.H., Coa, H. (1985). *Additional Reflection Plane Tests of Control Devices on an NACA 23024 Airfoil.* Wind Energy Report No. 23. Wichita, KS: Center for Energy Research Studies, Wichita State University.

Snyder, M.H.; Wentz, Jr., W.H., Coa, H. (1987). *Summary of Control Effectiveness of Vented Deflector-Ailerons.* Wind Energy Report No. 32. Wichita, KS: Center for Energy Research Studies, Wichita State University.

Toll, T.A.; Ivey, M.F. (1945). *Wind-Tunnel Investigation of a Rectangular NACA 2212 Airfoil With Semispan Ailerons and With Nonperforated, Balanced Double Split Flaps for Use As Aerodynamic Brakes.* Wartime Report L-56. Washington, D.C.: National Advisory Committee for Aeronautics (NACA).

Wayman, T.R. (1993). "Vented and Deflected Aileron for Aerodynamic Control of Power Modulation and Braking of Horizontal-Axis Wind Turbines". M.S. thesis, Wichita, KS: Wichita State University.

Appendix: Supplemental Data

Lift, Drag, and Moment Coefficient Data

Magnetic media containing airfoil angle of attack, lift, drag, and moment coefficient data for each control configuration examined can be obtained from the author. The files, written on an IBM-compatible personal computer formated disk, are in standard ASCII format.

Table 2 defines the file names for the various model configurations examined. Each file is composed of rows of four numbers that are comma delimited. The test angle of attack, lift coefficient, drag coefficient, and section quarter-chord moment coefficient are shown, respectively, on each row. The drag data in each file have been corrected for wind tunnel tare and interference effects, using an assumed constant tare and interference drag level of 0.020 for each configuration.

A portion of a typical data file (AS01.dat) follows.

-6.1,-1.3156,0.7133,0.269
-3.1,-1.6803,0.5407,0.2309
-0.1,-1.6027,0.4302,0.2012
3,-1.3902,0.4387,0.1949
5.8,-1.1937,0.4613,0.1935
9.1,-0.9711,0.4685,0.1807
11.9,-0.7807,0.4972,0.1765
15,-0.5662,0.5057,0.1648
17.9,-0.3581,0.519,0.1561
21,-0.0894,0.5179,0.1287
24,0.7992,0.4323,-0.0804
27,1.2546,0.3849,-0.1999

Referring to the numbers in the first row, the angle of attack is -6.1°, the lift coefficient is -1.3156, the drag coefficient is 0.7133, and the section quarter-chord coefficient is 0.269. Each row in a data file is read in the same fashion.

Table 2. Data disk file names for each test configuration.

CONFIGURATION or SUBCONFIGURATION	FILE NAME
NACA Double Split-Flap/60, 0/40	NSB00.DAT
NACA Double Split-Flap/60, 5/35	NSB01.DAT
NACA Double Split-Flap/60, 10/30	NSB02.DAT
NACA Double Split-Flap/60, 20/20	NSB03.DAT
NACA Double Split-Flap/60, Top 4.4/20, Bottom 4.4/20	NSB04.DAT
NACA Double Split-Flap/60, Top 4.4/20, Bottom 8.9/20	NSB05.DAT
NACA Double Split-Flap/60, Top 4.4/20, Bottom 14.4/20	NSB06.DAT
NACA Double Split-Flap/60, Top 0.0/20, Bottom 14.4/20	NSB07.DAT
NACA Double Split-Flap/60, Top 8.9/20, Bottom 14.4/20	NSB08.DAT
NACA Double Split-Flap/60, Top 14.4/20, Bottom 14.4/20	NSB09.DAT
NACA Double Split-Flap/112 (Clam-Shell), 5/15	CS00.DAT
NACA Double Split-Flap/112 (Clam-Shell), Top 5/20, Bottom 5/15	CS01.DAT
NACA Double Split-Flap/112 (Clam-Shell), Top 5/20, Bottom 5/20	CS02.DAT
NACA Double Split-Flap/112 (Clam-Shell), Top 5/15, Bottom 5/20	CS03.DAT
Smooth-Shoulder, (Basic Model), Delta= 0	SS00.DAT
Smooth-Shoulder, (Basic Model), Delta= -10	SS10.DAT
Smooth-Shoulder, (Basic Model), Delta= -30	SS30.DAT
Smooth-Shoulder, (Basic Model), Delta= -60	SS60.DAT
Smooth-Shoulder, (Basic Model), Delta= -90	SS90.DAT
Smooth-Shoulder, LE Stall Strip, Delta= 0	SSL00.DAT
Smooth-Shoulder, LE Stall Strip, Delta= -10	SSL10.DAT
Smooth-Shoulder, LE Stall Strip, Delta= -30	SSL30.DAT
Smooth-Shoulder, LE Stall Strip, Delta= -60	SSL60.DAT
Smooth-Shoulder, LE Stall Strip, Delta= -90	SSL90.DAT
Smooth-Shoulder, VG's, Delta= 0	SSV00.DAT
Smooth-Shoulder, VG's, Delta= -10	SSV10.DAT
Smooth-Shoulder, VG's, Delta= -30	SSV30.DAT
Smooth-Shoulder, VG's, Delta= -45	SSV45.DAT
Spoiler-Flap, (Basic Model), Delta = 0	SF00.DAT
Spoiler-Flap, (Basic Model), Delta = +10	SF10.DAT
Spoiler-Flap, (Basic Model), Delta = +30	SF30.DAT
Spoiler-Flap, (Basic Model), Delta = +60	SF60.DAT
Spoiler-Flap, (Basic Model), Delta = +90	SF90.DAT
Spoiler-Flap, Rough, Delta = 0	SFR00.DAT
Spoiler-Flap, Rough, Delta = +30	SFR30.DAT
Spoiler-Flap, Rough, Delta = +45	SFR45.DAT
Spoiler-Flap, Rough, Delta = +60	SFR60.DAT
Spoiler-Flap, Rough, Delta = +90	SFR90.DAT
Negative-Camber, (Basic Model), Delta= 0	NC00.DAT
Negative-Camber, (Basic Model), Delta= -10	NC10.DAT
Negative-Camber, (Basic Model), Delta= -30	NC30.DAT
Negative-Camber, (Basic Model), Delta= -60	NC60.DAT
Negative-Camber, (Basic Model), Delta= -90	NC90.DAT
Airfoil-Spoiler, Full Span, 0/40	AS01.DAT
Airfoil-Spoiler, 3/4 Span Spoiler, 0/40	AS02.DAT
Airfoil-Spoiler, 1/2 Span Spoiler, 0/40	AS03.DAT

REPORT DOCUMENTATION PAGE

Form Approved
OMB NO. 0704-0188

	2. REPORT DATE	3. REPORT TYPE AND DATES COVERED
	February 1995	Subcontract Report

TITLE AND SUBTITLE

Experimental Investigation of Aerodynamic Devices for Wind Turbine Rotational Speed Control Phase 1

5. FUNDING NUMBERS

C: XAD-3-133365-01

TA: WE418310

AUTHOR(S)

L. Scott Miller, Ph.D.

PERFORMING ORGANIZATION NAME(S) AND ADDRESS(ES)

National Institute for Aviation Research
Dept. of Aerospace Engineering
Wichita State University
Wichita, Kansas 67260-0044

8. PERFORMING ORGANIZATION REPORT NUMBER

SPONSORING/MONITORING AGENCY NAME(S) AND ADDRESS(ES)

National Renewable Energy Laboratory
1617 Cole Blvd.
Golden, CO 80401-3393

10. SPONSORING/MONITORING AGENCY REPORT NUMBER

TP-441-6913

DE95004034

1. SUPPLEMENTARY NOTES

NREL Technical Monitor: P. Migliore

2a. DISTRIBUTION/AVAILABILITY STATEMENT

12b. DISTRIBUTION CODE

UC-1211

3. ABSTRACT *(Maximum 200 words)*

An investigation was undertaken to identify the aerodynamic performance of five separate trailing-edge control devices, and to evaluate their potential for wind turbine overspeed and power modulation applications. A modular two-dimensional wind tunnel model was constructed and evaluated during extensive wind tunnel testing. Aerodynamic lift, drag, suction, and pressure coefficient data were acquired and analyzed for various control configurations and angles of attack. To further interpret their potential performance, the controls were evaluated numerically using a generic wind turbine geometry and a performance analysis computer program. Results indicated that the Spoiler-Flap control configuration was best suited for turbine braking applications. It exhibited a large negative suction coefficient over a broad angle-of-attack range, and good turbine braking capabilities, especially at low tip-speed ratio.

4. SUBJECT TERMS

wind turbines—controls, braking, aerodynamic devices, wind tunnel blade testing, speed control

15. NUMBER OF PAGES

16. PRICE CODE

17. SECURITY CLASSIFICATION OF REPORT	18. SECURITY CLASSIFICATION OF THIS PAGE	19. SECURITY CLASSIFICATION OF ABSTRACT	20. LIMITATION OF ABSTRACT
Unclassified	Unclassified	Unclassified	UL